THESIS FOR THE DEGREE OF DOCTOR OF PHILOSOPHY

Hydrogen Production by Integration of Fluidized Bed Heat Exchangers in Steam Reforming

VIKTOR STENBERG

Department of Space, Earth and Environment
CHALMERS UNIVERSITY OF TECHNOLOGY
Gothenburg, Sweden 2020

Hydrogen Production by Integration of Fluidized Bed Heat Exchangers in Steam Reforming

VIKTOR STENBERG
ISBN 978-91-7905-393-2

Doktorsavhandlingar vid Chalmers tekniska högskola
Ny serie nr 4860
ISSN 0346-718X

Department of Space, Earth and Environment
Chalmers University of Technology
SE-412 96 Gothenburg
Sweden
Telephone + 46 (0) 31 772 1000

Printed by Chalmers Reproservice
Gothenburg, Sweden 2020

Hydrogen Production by Integration of Fluidized Bed Heat Exchangers in Steam Reforming

VIKTOR STENBERG
Division of Energy Technology
Department of Space, Earth and Environment
Chalmers University of Technology
SE-412 96 Gothenburg, Sweden

Abstract

The possibility to integrate fluidized beds as heat sources for steam reforming in industrial hydrogen production plants is examined in this work. The processes proposed include traditional catalytic steam reforming of natural gas (SMR), with downstream shift reactors and purification steps; the main difference is the reformer furnace. The conventional SMR plant includes a gas-fired furnace where the heat necessary for the endothermic steam reforming reaction is generated by combustion of gaseous fuels and transferred to the steam reforming tubes mainly by radiation. The alternative which is investigated in this work is to immerse the reformer tubes in fluidized bed heat exchangers (FBHE) with the potential of improved heat transfer to the reformer tubes and in some cases provide inherent CO_2 capture. Several concepts have been studied using a combination of thermodynamic and techno-economic evaluations as well as experiments in fluidized beds at laboratory and semi-industrial scale.

The first of the proposed process consists of a single fluidized bed heat exchanger where the fuel is converted in the bed using oxygen carrier particles. This makes it possible to reduce the supplementary fuel consumption of natural gas, which results in a reduction of CO_2 emissions from the plant by 11.6%. The levelized hydrogen production cost is approximately 7% lower in comparison with the conventional SMR plant. Lab-scale experiments were performed where inert silica sand was compared with two oxygen carriers using methane and PSA off-gas as fuel. The experiments showed that the fuel was converted in the dense bed even at moderate furnace temperatures (i.e., 600-800˚C) and the use of oxygen carrier increased the fuel conversion in the bed. The experiments suggested that the proposed principle is feasible.

The second proposed process is based on integration of SMR with chemical-looping combustion, a novel process which involves the use of an oxygen carrier is circulated between two interconnected fluidized bed reactors. In this plant the flue gas stream obtained from the fuel reactor is not diluted with N_2 resulting in that the CO_2 produced can easily be captured. The supplementary fuel consumption increases only slightly compared to the first proposed configuration. It presents a hydrogen production efficiency which is 7.7% higher than the conventional SMR plant. The levelized production cost is only around 1% lower than for the conventional plant, even though it includes CO_2 capture and CO_2 compression.

The third proposed configuration is also based on chemical-looping combustion but uses biomass instead of natural gas as supplementary fuel, which enables the possibility to achieve net negative

emissions. The estimated net CO_2 emissions corresponds to a reduction by 142% compared to the conventional SMR plant, at a levelized hydrogen production cost which is only 1.4% higher. The hydrogen production efficiency is 2.1% higher than for the conventional plant.

The experimental campaigns on bed-to-tube heat transfer and oxygen carrier aided combustion support the claim that fluidized bed heat exchangers are suitable for use in the proposed SMR application, since the estimated heat transfer coefficient from bed-to-tube is above 500 W/(m^2K)). In the techno-economic assessment it is observed that the proposed configuration display high thermal efficiency and the possibility to achieve significant reductions in CO_2 emissions in industrial hydrogen production. All three proposed processes are well worth considering for real world applications. They could provide several environmental benefits and this work could be used as a support for further developments towards industrial implementation.

Keywords: steam reforming, fluidized bed heat exchanger, oxygen carrier aided combustion, chemical-looping combustion, bed-to-tube heat transfer.

List of publications

This thesis is based on the following papers, which are referred to in the text by their Roman numerals:

Paper I Stenberg V, Rydén M, Mattisson T, Lyngfelt A. Exploring novel hydrogen production processes by integration of steam methane reforming with chemical-looping combustion (CLC-SMR) and oxygen carrier aided combustion (OCAC-SMR). *International Journal of Greenhouse Gas Control.* 2018;74:28-39.

Paper II Stenberg V, Spallina V, Mattisson T, Rydén M. Techno-economic analysis of H2 production processes using fluidized bed heat exchangers with steam reforming – Part 1: Oxygen carrier aided combustion. International Journal of Hydrogen Energy. 2020; 45: 6059-6081.

Paper III Stenberg V, Spallina V, Mattisson T, Rydén M. Techno-economic analysis of H2 production processes using fluidized bed heat exchangers with steam reforming – Part 2: Chemical-looping combustion. *Submitted for publication.*

Paper IV Stenberg V, Rydén M, Mattisson T, Lyngfelt A. Experimental investigation of Oxygen Carrier Aided Combustion (OCAC) of Methane and PSA off-gas. *Submitted for publication.*

Paper V Stenberg V, Sköldberg V, Öhrby L, Rydén M. Evaluation of bed-to-tube surface heat transfer coefficient for a horizontal tube in bubbling fluidized bed at high temperature. Powder Technology. 2019; 352: 488-500.

Paper VI Stenberg V, Lind F, Rydén M. Measurement of bed-to-tube surface heat transfer coefficient to a vertically immersed U-tube in a bubbling loop seal of a CFB boiler. *Submitted for publication.*

Author details

Viktor Stenberg is the principal author of **Papers I−VI** and was responsible for planning and conceptualization of work, implementation, analysis and writing. Professor Tobias Mattisson contributed with discussion and critical review of **Papers I-IV**. Professor Anders Lyngfelt contributed to discussion and editing of **Papers I & IV**. Dr Vincenzo Spallina contributed to the development of the Aspen Plus simulation model in **Papers II-III** as well as discussion and editing of these papers.

M.Sc Lovisa Öhrby contributed to the experimental work of **Paper V**. M.Sc Viktor Sköldberg contributed to the experimental work, discussion and editing of **Paper V**. Docent Fredrik Lind contributed with ideas, discussion and editing of the work with **Paper VI**. Professor Magnus Rydén contributed ideas, discussion, and editorial support for all six papers.

Related publications not included in the thesis:

A. Stenberg V, Rydén M, Mattisson T, Lyngfelt A. Hydrogen production by integration of steam reformation with chemical-looping combustion, *4th International Conference on Chemical Looping, September 26-28, 2016, Nanjing, China*.

B. Stenberg V, Rydén M, Mattisson T, Lyngfelt A. Combustion of Methane in Bubbling Fluidized Bed with Oxygen Carrier Aided Combustion (OCAC), *23rd International Conference on Fluidized Bed Conversion, Seoul, Korea, May 13-17, 2018*.

C. Aronsson J, Krymarys E, Stenberg V, Mattisson T, Lyngfelt A, Rydén M. Improved Gas-Solids Mass Transfer in Fluidized Beds: Confined Fluidization in Chemical-Looping Combustion. Energy & Fuels. 2019;33: 4442-4453.

D. Kumar T R, Mattisson T, Rydén M, Stenberg V. Process Analysis of Chemical Looping Gasification of Biomass for FT-crude Production with Net-Negative CO2 Emissions. *Submitted for publication.*

E. Nemati N, Andersson P, Stenberg V, Rydén M. The Effect of Random Packings on Heat Transfer and particle segregation in Packed-Fluidized-Bed. *Submitted for publication.*

List of abbreviations

AFR	Air-to-fuel ratio
AR	Air reactor
BEC	Bare Erected Cost
BFB	Bubbling fluidized bed
BIO	Biomass
BUA	Bottom-up approach
C28	Mn-based perovskite structure oxygen carrier material, $CaMn_{0.775}Mg_{0.1}Ti_{0.125}O_{3-\delta}$
CAGR	Compound annual growth rate
CCA	Cost of CO_2 avoidance
CEPCI	Chemical Engineering Plant Cost Index
CFB	Circulating fluidized bed
CCF	Capital charge factor
CLC	Chemical-looping combustion
COP21	2015 United Nations Climate Change Conference held in Paris
FBHE	Fluidized bed heat exchanger
FCEV	Fuel Cell Electric Vehicle
FR	Fuel reactor
GFF	Gas-fired furnace
GHG	Greenhouse gas emissions
H_{bed}	Bed height
HX	Heat exchanger
HYBRIT	Joint venture aiming at substituting coal with hydrogen in steel production
LCOH	Levelized cost of hydrogen
LD slag	Steel converter slag from the Linz-Donawitz process
LHV	Lower heating value
O&M	Operations and maintenance
OCAC	Oxygen carrier aided combustion
MP	Measurement point
NDIR	Nondispersive infrared sensors
NG	Natural gas
PSA	Pressure swing adsorption
S/C ratio	Steam-to-carbon ratio (molar basis)
SMR	Steam methane reforming
SUCCESS	Research project aimed for scale-up of CLC oxygen carrier production
TPC	Total plant cost

Nomenclature

A_i	Tube inside surface area
A_o	Tube outside surface area
C	Equipment cost with the capacity S
C_o	Reference cost of equipment with reference capacity S_0
d_p	Weighted mean particle diameter based on sieving

E_{CO2}	Specific CO_2 emissions from the plant
δ	Degree of oxygen deficiency
e_p	Emissivity of particles
e_b	Emissivity of bed (= $0.5(1+e_p)$)
e_s	Emissivity of tube surface
ε	Voidage in fluidized bed
ε_{BFB}	Voidage in bubbling fluidized bed
ε_{fixed}	Voidage in fixed bed (assumed to be equal to 0.4)
H	Height in OCAC reactor
h_i	Tube inside heat transfer coefficient
h_o	Bed-to-tube surface (or outside) heat transfer coefficient
h_{rad}	Radiative contribution to the outside heat transfer coefficient
h_w	Heat transfer coefficient through the tube wall
k_w	Thermal conductivity of tube wall
$\dot{m}$	Mass flow
$\dot{m}_{biomass}$	Mass flow of biomass used as supplementary fuel
$\dot{m}_{NG,eq}$	Equivalent mass flow of NG to the process including feed and supplementary fuel
$\dot{m}_{NG,eq,bio}$	Equivalent mass flow of NG for the biomass to the process
$\dot{m}_{NG,tot}$	Total flow of NG to the process including feed and supplementary fuel
$\dot{M}$	Molar flow
n	Scale factor in economic calculations
$\eta_{el,ref}$	Efficiency of reference plant for electricity production
$\eta_{th,ref}$	Efficiency of reference plant for heat production
η_{H2}	Hydrogen production efficiency
η_{eq,H_2}	Equivalent hydrogen production efficiency
η'_{eq,H_2}	Equivalent hydrogen production efficiency based on that only electricity export is possible
P	Pressure
Q	Heat load delivered in FBHE experiment
Q_{th}	Heat delivered from steam export
ρ_b	Poured bulk density
ρ_g	Gas density
ρ_p	Particle density (= $\rho_b/(1-\varepsilon_{fixed})$)
S	Capacity (scaling parameter in cost functions)
S_o	Capacity for reference equipment
σ	Stefan Boltzmann constant (=$5.67*10^{-8}$ W/(m^2K^4))
T_b	Bed temperature
T_{fg}	Reformer furnace flue gas temperature
$T_{s,i}$	Tube inside surface temperature (°C)
$T_{s,o}$	Tube outside surface temperature (°C)
T_{water}	Mean water temperature in the tube (°C)
u_{mf}	Minimum fluidization velocity
u_t	Terminal velocity
U	Overall heat transfer coefficient
W_{el}	Net electricity production
$Y_{H2,WGS}$	Hydrogen yield after water-gas shift reactors
z	Number of units

Acknowledgement

I have always sought challenges which I myself and others around me consider to be difficult. Pursuing a PhD is one of those challenges. You are many who have made it possible for me to take on this PhD adventure and this section is an opportunity for me to recognize these people.

First, I want to thank those involved at the division of Energy Technology at Chalmers. I am very thankful to my main supervisor Magnus Rydén who has been a great support both when things go well to discuss plans for future work but perhaps even more so when you are able to calm me down when things do not go as well. I would also like to thank Tobias Mattisson and Anders Lyngfelt for interesting discussions and most valuable input. Henrik Leion should also be recognized for being the one which gave me the opportunity to pursue a master thesis within the world of oxygen carriers. I would also like to thank Rustan Hvitt, Jessica Bohwalli, Johannes Öhlin, Fredrik Lind and Ulf Stenman for helping me with setting up the experimental activities in the new reactor system and in the Chalmers Power Central. I have learned a lot from the discussions with you which has been very valuable when planning my experimental work. Every single colleague at Energy technology should be thanked for contributing to a fantastic working environment. I have had so many exciting discussions with you both unrelated and related to work which I have enjoyed very much. A special thanks to Holger for being a great office roommate with whom I have shared both laughs, kombucha brewing and interesting discussions.

Secondly, I would also like to send some well-deserved thanks to some people outside Sweden who have been involved in this work. I am happy for the interesting discussions I have shared with Martin Østberg, Morten Boberg Larsen and Francois-Xavier Chiron at Haldor Topsøe during our project meetings. I am most thankful to Vincenzo Spallina for providing the opportunity to conduct part of my PhD in the Netherlands with the research group of Chemical Process Intensification at the Technical University of Eindhoven (TU/e). I also want to thank the rest of the research group at TU/e for making my stay in Eindhoven so stimulating!

Working on this research topic has allowed me to work with many different research areas and there are so many of you who have contributed to this work indirectly through sharing thoughts and ideas with me on various topics, thus the notion “none mentioned, none forgotten” applies very much. I want to thank my beloved family and friends for all the support in my ambitions at and outside of work. And my dear Louise, thank you for being by my side and bringing me so much joy, I’m looking forward to our future together.

This work has been supported by the Swedish Energy Agency (project 40559-1 - Heat to endothermic industrial processes with new efficient combustion method in fluidized bed).

Viktor Stenberg

Gothenburg, November 2020

Table of contents

1. Introduction

In the 18th century the industrial revolution began which marked the transition from a society based on agriculture and hand production methods to machine manufacturing. This revolution led to rapid technological, economic and population growth as well as a growth in energy consumption, with coal becoming the dominating energy source during the first part of the 20th century [1]. During the latter part of the 20th century a diversification of fossil energy consumption was observed, where use of crude oil and natural gas came to play an important role as well [1]. At the same time, the energy demand increased rapidly, leading to an increase in greenhouse gas (GHG) emissions. GHG emissions, of which carbon dioxide is the major contributor, has been linked to the increase in average global temperature. Fossil fuel consumption corresponded to 87% of the global primary energy consumption in 2017 [1]. At the COP21 conference in Paris in 2015 an international agreement was made to limit global warming to well below 2˚C compared to pre-industrial levels and attempt to limit the temperature increase to 1.5˚C. The IPCC special report on a global warming of 1.5˚C discusses the carbon budget to limit the global warming within the 1.5˚C target. Virtually all the emission scenarios overshoot a 1.5˚C temperature increase but is compensated by future negative emissions [2]. It seems clear that significant emissions reductions are required in all sectors and it is probable that also large-scale deployment of negative emissions technologies is required, to have a chance to limit the global warming to 1.5˚C.

The chemical industry is one of the sectors where significant reductions in CO_2 emissions are required. One of the most important chemical products today is hydrogen. Hydrogen is mostly used for production of fertilizers and methanol, in oil refining and metallurgical industries. The annual hydrogen production corresponds to approximately 2% of the primary energy demand [3, 4]. Approximately 95% of the hydrogen produced today is based on fossil fuels [3] and hydrogen production accounts for more than 1% of the global CO_2 emissions [5], approximately 500 Mton CO_2 per year. Hydrogen production based on fossil fuels is considered to be the most economically feasible alternative during the next 20 years and it could also play an important role in the longer term, i.e. 20-50 years [6]. The two main production routes are steam reforming of methane/natural gas and reforming of oil/naphtha, which account for 48% and 30% of the global hydrogen production, respectively [7]. The two routes involve similar processes, the main difference being the fuel used. The rest is produced from coal gasification, 18% and electrolysis, 4% [5]. Large-scale SMR production is recognized as benchmark technology for hydrogen production today based on its general economic feasibility globally [5].

The Compound Annual Growth rate (CAGR) for hydrogen is expected to exceed 6% from 2016 to 2022 [5]. It is mainly driven by legislation to regulate desulfurization of petroleum products and increased demand for hydrogen in the transportation sector where hydrogen can be used either directly or indirectly through use of biofuels which require hydrogen in the refinery production process. Hydrogen is of interest as transportation fuel since it can be used in fuel cell vehicles which are quiet, energy efficient and cause zero emissions. The deployment of fuel cell electric vehicles is at present limited, around 7000 vehicles on the roads in 2017 [8], but could increase

significantly. The Hyundai Motor Group has, for example, announced that they aim to produce 700 000 fuel-cell systems annually by 2030 which includes 500 000 units for Fuel Cell Electric Vehicles (FCEV) [9].

Another interesting initiative is the HYBRIT project by SSAB, LKAB and Vattenfall. The aim of this project is to replace coal with hydrogen in the steel-making process [10]. The steel industry is a major contributor to CO_2 emissions both globally, around 7%, and in Sweden, approximately 10%. This is another example of a potential source for increased demand for hydrogen in the future.

Based on the expected future demand for hydrogen, it is important to target sustainable hydrogen production processes. As presented above, the most common hydrogen production method today is steam reforming. This process is commonly composed of a reformer, a shift reactor and a hydrogen purification system based on pressure swing adsorption (PSA). The key component in this system is the reformer where steam and hydrocarbons react at high temperature and high pressure inside reactor tubes, in presence of a catalyst. The steam reforming reaction is endothermic, and the heat required for the reaction is provided by external heating of the tubes in a reformer furnace. The syngas produced in the reformer is fed to a shift reactor where additional hydrogen is produced. This stream is then treated in a PSA unit where a product stream of high purity hydrogen is produced, as well as an off-gas containing CO, H_2, CH_4 and CO_2. The off-gas is commonly used as fuel in the reformer furnace. In addition to the off-gas, supplementary fuel is introduced to the furnace to provide the heat necessary for the steam reforming reaction, see the "Old reformer" in Figure 1.

One approach to achieve a reduction of the CO_2 footprint in hydrogen production is to find a process which can provide a higher hydrogen production efficiency. This would mean reduced supplementary fuel consumption and therefore a reduced fossil fuel input to the process per unit of hydrogen produced. The supplementary fuel consumption can for example be reduced by improving the heat transfer to the reformer tubes, which would allow for reduced furnace temperature and improved hydrogen production efficiency. In order to improve the heat transfer to the reformer tubes the gas-fired furnace (GFF) could be replaced with a single fluidized bed heat exchanger where the reformer tubes are immersed in the fluidized bed of oxygen carrier particles [11]. The concept is illustrated in Figure 1.

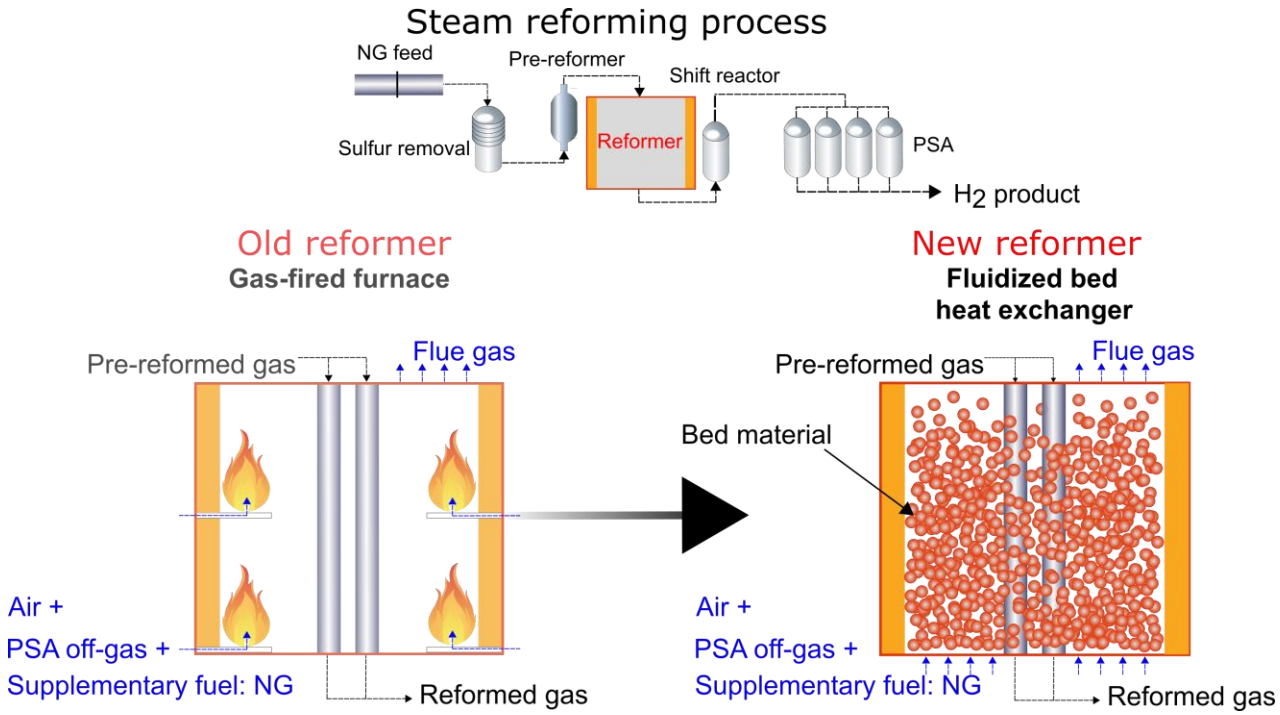

***Figure 1**: Illustration of the concept to replace the gas-fired furnace with a fluidized bed heat exchanger.*

In order to reach close to net zero CO_2 emissions from a plant based on the SMR process with externally heated reformer tubes it would be possible to integrate the process with either post-combustion capture technologies [12] or chemical-looping combustion (CLC) for inherent CO_2 capture [13]. Chemical-looping has been identified as one of the most promising options to obtain a low incremental cost for CO_2 capture [14]. One of the key reasons for this is that it has a low energy penalty compared to most of the other capture technologies, such as for example post-combustion capture by amines, and ideally no cost of CO_2 separation [14]. The option to integrate SMR with CLC was first proposed by Rydén and Lyngfelt [13]. In this work and in articles presented by other authors [11, 15, 16], the feasibility of the process based on thermodynamics has been presented and the estimated efficiencies are competitive with conventional steam reforming without CO_2 capture. Spallina et al. [15] also estimated the hydrogen production cost for this option, which was competitive with conventional SMR. Other chemical-looping based alternatives for hydrogen production which are not based on externally heated reformer tubes are reviewed by Adánez et al. [14], Abad [17] and Luo et al. [18].

In order to achieve a H_2 production process with net negative CO_2 emissions it could be possible to use biomass instead of fossil fuel as supplementary fuel to the CLC system integrated with SMR [11, 19]. Net negative emissions can be obtained since the carbon present in the biomass originates from CO_2 which has been withdrawn from the atmosphere through photosynthesis. Some new challenges are added, which are mainly connected to the risk of melting/slagging of biomass ash which could cause deposit formation on the reformer tubes if these tubes would be placed in the fuel reactor of the CLC system. In the cited study [11] the reformer tubes were placed in an external fluidized bed heat exchanger, but the air reactor could be another possibility as suggested in [19]. It should be mentioned that the gasified biomass volatiles could potentially

also be used as feed to the reformer tubes with commercial steam reforming catalysts. However, this brings several additional challenges; for example, catalyst poisoning due to impurities such as sulphur, tar and alkali species [20, 21]. This option is not considered in this work.

1.1. Aim of the thesis

The aim of this thesis is to evaluate the potential to use fluidized bed heat exchangers as heat source in steam reforming plants for hydrogen production. In order to gain a comprehensive view of the technology, different aspects were studied, including process simulations and experimental endeavours in fluidized beds. The thesis encompasses the main findings of six papers, all of which cover different aspects to assess the potential for industrial implementation of the processes proposed. Additional details for each of these investigations can be found in the appended papers.

Papers I-III evaluate the thermodynamic performance of processes where fluidized bed heat exchangers are integrated in steam reforming plants for hydrogen production. **Papers II-III** present a more detailed evaluation of the thermodynamic performance as well as an economic analysis of industrial scale hydrogen production plants. **Paper II** focuses on integration with a single fluidized bed heat exchanger in the SMR plant with an oxygen carrier as bed material for in-bed fuel conversion, in accordance to the principle examined experimentally in **Paper IV**. **Paper III** investigates the integration of SMR with chemical-looping combustion. **Paper IV** investigates oxygen carrier aided combustion, i.e. the possibility to increase the in-bed fuel conversion using oxygen carriers as bed material in a lab-scale bubbling fluidized bed (BFB) reactor. The fuels used are PSA off-gas which makes up a large part of the fuel in the conventional steam reformer furnace and methane which is considered to be a key component in the off-gas. **Paper V** investigates experimentally the bed-to-tube surface heat transfer at high bed temperatures for three different bed materials of various sizes. The heat transfer coefficients determined are compared to heat transfer correlations which could be used to predict the heat transfer to the steam reformer tubes in the proposed applications, which have been used in **Paper II-III**. **Paper VI** also evaluates the bed-to-tube heat transfer, but in a semi-industrial scale circulating fluidized bed (CFB) boiler where a vertical U-tube is immersed into one of the loop seals. Different fluidization gases, bed materials, tube bundle orientations and circulation rates for example were evaluated.

Figure 2 illustrates the connection between the papers graphically.

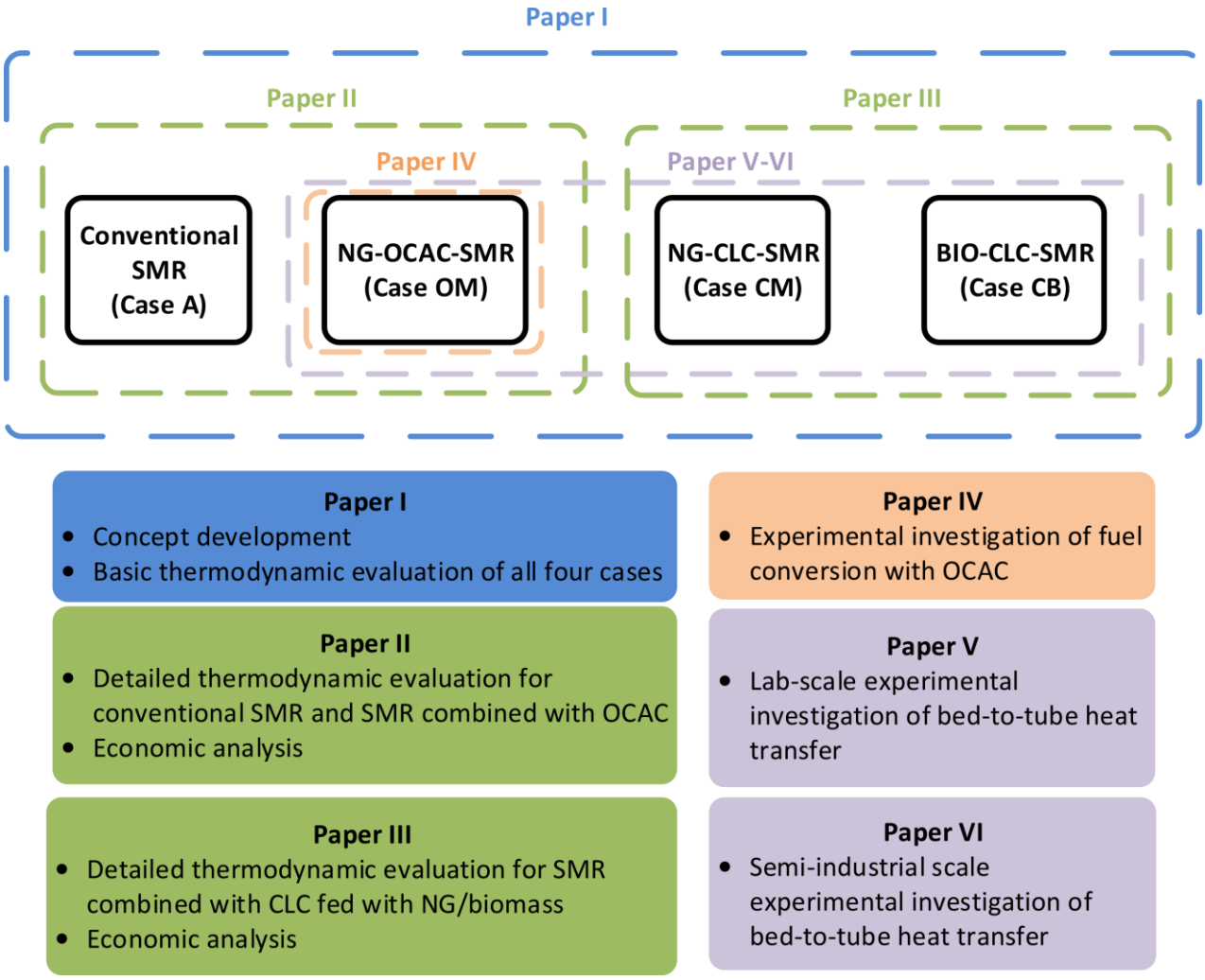

***Figure 2**: Illustration of the areas studied in the papers included in this thesis. SMR=Steam methane reforming, OCAC=Oxygen carrier aided combustion, CLC=Chemical-looping combustion, NG=Natural gas and BIO=Biomass.*

1.2. Outline of the thesis

The thesis is organized as follows. The introduction is followed by Chapter 2 which provides a review of the literature describing conventional SMR technology as well as three key technologies related to the proposed processes. Chapter 3 presents the experimental setups consisting of reactors and materials used in the experiments in **Papers IV-VI**. Chapter 4 presents the methodology used in the six papers where key assumptions in the presented models and the methods used in the experimental campaigns are described. Chapter 5 presents the main results and discusses the contribution of the individual results to the overall aim of this thesis. The main conclusions of this thesis are presented in Chapter 6. Additional reflections about this thesis work as well as suggestions for future studies are presented in Chapter 7.

2. Background

2.1. Steam Methane reforming

The conventional steam methane reforming (SMR) process is based on catalytic reforming of natural gas at high temperature, 800-950˚C and high pressure, 15-40 bar. The endothermic reaction, see Eq.(1), takes place in high-alloy reformer tubes where a catalyst, typically nickel-based [22] is supported on pellets [23]. The tubes are heated by external gas burners hosted in a furnace, where different tube and burner arrangements can be used [23].

$$CH_4 + H_2O \rightleftharpoons CO + 3\,H_2 \quad \Delta H_0^{298K} = 206.2\ \text{kJ/mol} \tag{1}$$

The reformer is followed by one or more water-gas-shift (WGS) reactors to adjust the H_2/CO-ratio, which in ammonia and hydrogen production plants should be as high as possible [23]. CO is converted according to the equilibrium-limited and slightly exothermic WGS reaction, see Eq.(2), which is favoured by low temperatures.

$$CO + H_2O \rightleftharpoons CO_2 + H_2 \quad \Delta H_0^{298K} = -41.2\ \text{kJ/mol} \tag{2}$$

Product gas formed in the shift reactor is cooled to close to ambient temperature and sent to a pressure swing absorber (PSA) where a high purity hydrogen stream is obtained, i.e., up to 99.999% purity [24]. A low pressure off-gas stream is generated which is rich in CO_2, but which also contains combustible gases in form of CO, CH_4 and H_2. The off-gas is typically fed as fuel to the reformer furnace [24], together with supplementary fuel in form of natural gas. Combustion of off-gas and natural gas provides the heat for the endothermic reaction Eq.(1).

SMR plants typically generate significant amounts of excess heat which in general should be minimized or avoided [23], since it results in high fuel consumption to produce a product with low value. One of the main reasons for the excess heat generation is the rather low heat transfer coefficient to the reformer tube surface, which constitutes the primary bottle neck for conversion of methane to synthesis gas. The driving force for heat transfer is mainly radiation, which requires combustion at very high temperatures in order to be sufficiently effective in transferring the required heat [25]. Operation with a relatively low heat transfer coefficient results in a need for high furnace temperature, which in turn results in a flue gas with more latent energy content than what can realistically be used internally within the process, i.e. excess heat production. The high temperatures which are required also results in thermal NO_x emissions. If the heat transfer to the tube wall could be improved a lower furnace temperature could be used, since the heat transfer to the tube wall from the outside is typically the rate limiting step for reaction (1). This would lead to the following results: i) reduced supplementary fuel consumption, ii) reduced excess heat generation, iii) reduced thermal NO_x emissions, iv) reduced risk of temperature hotspots on the tube surface, a common reason for reformer tube failure, which is caused by uneven heat flux to the reformer tubes and is difficult to control by flame combustion.

2.2. Chemical-looping combustion

Chemical-looping combustion (CLC) is a process which can be used for heat and power production while also providing inherent CO_2 capture. The CLC system, see Figure 3, consists of two reactor vessels, typically interconnected fluidized beds, and a solid oxygen carrier. In the air reactor the reduced oxygen carrier, Me_xO_{y-1}, is oxidized with air, Eq.(3). Here Me_xO_y is a generic oxygen carrier. In the fuel reactor oxygen is released from the oxygen carrier by a gas-solid reaction with the fuel, Eq.(4).

$$(2j + k)Me_xO_{y-1} + (j + 0.5k)O_2 \rightleftharpoons (2j + k)Me_xO_y \quad (3)$$

$$(2j + k)Me_xO_y + C_jH_{2k} \rightleftharpoons (2j + k)Me_xO_{y-1} + kH_2O + jCO_2 \quad (4)$$

By adding Eq.(3) and (4), the total heat evolved in the system is found, and this is equal to the heat released during normal combustion. Note that the oxygen is transported to the fuel reactor with the oxygen carrier, with the result that the flue gas stream from the fuel reactor is not diluted with N_2. Thus, the CO_2 can easily be separated from the flue gas by condensation of steam.

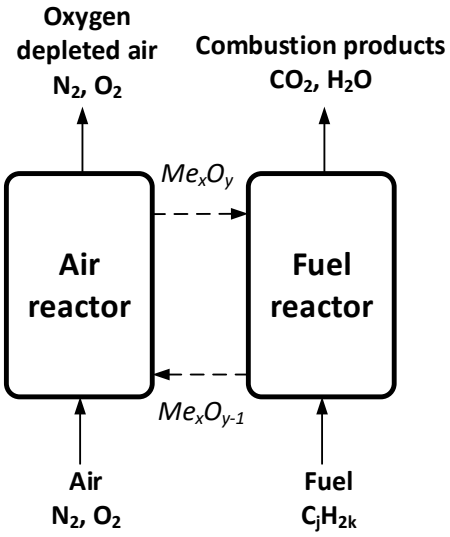

***Figure 3**: Schematic description of chemical-looping combustion of a generic hydrocarbon fuel.*

The energy balance of the two reactors depends on the oxygen carrier used, the temperature of the reactors and the fuel. While the oxidation of the oxygen carrier is always strongly exothermic, the reduction of the oxygen carrier may be either endothermic or exothermic. Synthetic particles based on Fe_2O_3 (hematite), NiO (nickel oxide), Mn_3O_4 (manganese oxide) and CuO (copper oxide) have commonly been used as oxygen carriers [13]. Oxygen carriers can also be ores and minerals such as ilmenite, an iron-titanium oxide, industrial by products containing metal oxides such as steel converter slag. It is also possible to manufacture combined oxide oxygen carriers using several raw materials such as the calcium-manganese-based material $CaMn_{0.775}Mg_{0.1}Ti_{0.125}O_{3-\delta}$, also called C28. The technical requirements may differ depending on the application, but the oxygen carrier should generally have good fluidization properties, have a high reactivity with fuel and air as well as having high mechanical integrity. A summary of the current research status for CLC can be found in recent review articles [14, 26-28].

2.3. Oxygen carrier aided combustion

Oxygen carrier aided combustion (OCAC) is a combustion technology which recently has been proposed and evaluated [29]. The fundamental idea is to replace the largely inert bed material used in fluidized bed boilers, typically silica sand in biomass boilers and waste incinerators, with an oxygen carrier similar to what is used in chemical-looping combustion (CLC). The presence of the oxygen carrier introduces new fuel conversion mechanisms and allows for the transport of oxygen in space and time [30, 31]. The oxygen carrier contains a metal-oxide which can undergo reduction and oxidation at the conditions in the fluidized bed combustion unit. The reactions are the same as presented in the previous section, Eq.(3) and (4).

The OCAC technology has been demonstrated in a 12 MW_{th} circulating fluidized bed boiler at Chalmers University of Technology which showed that the CO concentration in the flue gas leaving the boiler could be decreased by as much as 80% when using 40 wt.% ilmenite (a titanium-iron-ore), compared to operation with sand only [29]. Experiments with manganese ore and sand allowed for reduction with up to 70% for low air-to-fuel ratios [30]. Apart from minimizing emissions of carbon monoxide and unburnt hydrocarbons in conventional fluidized bed boilers, OCAC could also facilitate conversion of stable molecules such as methane in the dense zone of the fluidized bed. Because of the thermal inertia of the solids more stable fuel components, where methane is the most stable of all, do not easily burn in the dense bed, since the moderate temperature will effectively hinder ignition of the air-fuel mixture. This is not necessarily an issue in power plant since combustion will take place also in the freeboard above the dense bed, but if the goal is to provide heat directly to the fluidized bed solids, for immediate transfer to immersed reactor tubes, this phenomenon could create problems. This is because heat will be generated mostly above the bed. Thus, it will not be available where it is actually needed. The fuel used in the reformer furnace is a mix of mainly CH_4, CO and H_2 where CH_4 should be regarded as the most difficult fuel to oxidize.

CLC systems are examples of systems where complete conversion of methane/natural gas has been observed for several different oxygen carriers, i.e. under conditions without presence of air and at temperatures similar to the target temperature for this application [32-39]. It should also be mentioned that an oxygen carrier which is oxidized to a high extent is likely to have a higher reactivity, compared to an oxygen carrier that has been subject to reduction. Therefore, provided that the amount of bed material is sufficient in relation to the fuel flow, OCAC should allow for direct conversion of methane in the dense fluidized bed. The effect of OCAC was observed in a study where the performance of sand and the oxygen carrier Fe_2O_3 was compared in a bubbling fluidized bed system for combustion of methane at 700˚C. In this study it could be seen that essentially nothing happened inside the sand bed. But as soon as only 0.13-1.3% of the bed mass was substituted with Fe_2O_3, methane was converted to a great extent within the bed [40]. Experimental campaigns with ilmenite [29], manganese ore [30] and steel converter slag [41] in a 12 MW_{th} CFB boiler with wood chips as fuel all indicated that partial substitution of the silica sand bed with these bed materials increased fuel conversion and therefore also the heat generation in the dense bed. This was indicated by the temperature at the top of the dense bed [30, 41] being higher when oxygen carrier was present in the bed, compared to using only silica sand. Also, the

temperature drop in the cyclone [29, 30, 41] was more pronounced when oxygen carriers were present, strongly suggesting that much less fuel entered the cyclone.

CO and H_2 which are the other fuel gases present in the reformer furnace, due to their presence in the PSA off-gas, are known to be more readily converted in fluidized bed reactors and have higher reactivity with commonly used oxygen carriers [42, 43]. This motivates the focus on the methane being the rate-limiting component.

In this thesis, one of the proposed processes involves implementation of OCAC in a single bubbling fluidized bed, which provides a heat source for steam reforming where the steam reforming tubes are placed in the dense bed [11].

2.4. Fluidized bed heat exchanger

Fluidized beds are known to provide high heat transfer rates in the bed and almost uniform bed temperatures [44, 45]. As a result, there are many possible applications of fluidized beds as heat sources in general. One such approach is to use so called fluidized bed heat exchangers (FBHEs), which essentially consists of tubes with water/steam immersed in the dense zone of bubbling fluidized beds. FBHEs are commonly located for example after the cyclone in circulating fluidized bed (CFB) power plants, where the hot particles from the cyclone are cooled in contact with the tubes, see Figure 4.

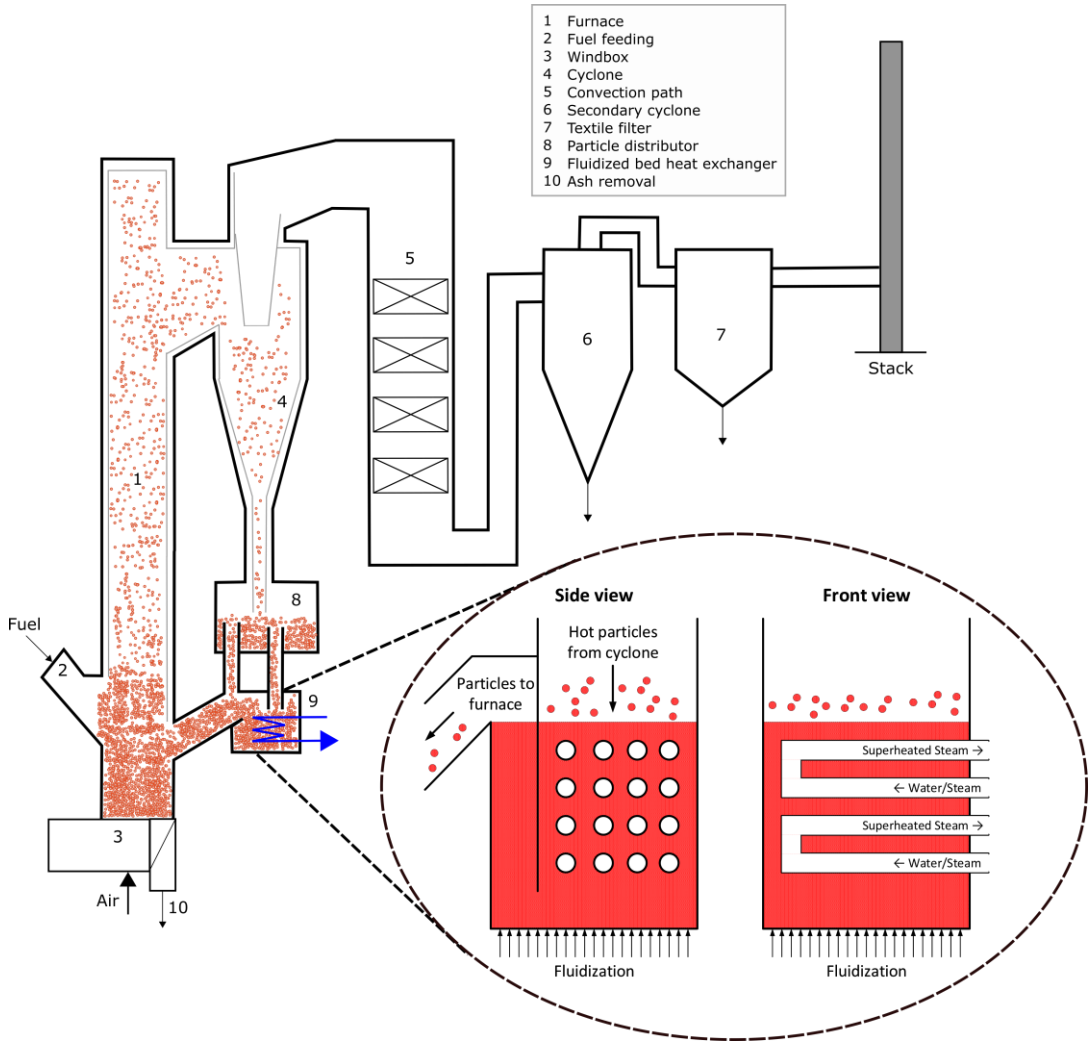

***Figure 4**: FBHE in circulating fluidized bed boiler.*

In boilers, the FBHEs are operated with a low superficial gas velocity, around 0.2-0.5 m/s to avoid tube erosion, with steam generation or superheating of steam taking place inside the tubes. These heat transfer surfaces improve the flexibility of the boiler significantly and can be used to control the superheat and reheat temperature, as well as the combustion temperature in the boiler. They can serve as an alternative to heat exchange surfaces inside the furnace or in the convection section [46]. Despite the favourable characteristics of fluidized bed heat exchangers, the use of FBHE at elevated temperature levels has so far been limited to water/steam-mixtures in immersed tubes for steam production. There are currently, to the best of the author's knowledge, no examples of implementations of FBHEs as a heat source for tubular chemical reactors. Using FBHEs as a heat source for steam reforming should be a most interesting possibility since it would be possible to achieve significantly improved conditions for heat transfer to the reformer tubes.

There are several models that describes the heat transfer between a fluidized bed and a surface, one of them being the packet-renewal model [47]. According to this model, packets of particles are swept into contact with the heat transfer surface for a short period of time by the movements of bubbles. The first layer of particles in contact with the surface will cool down, or heat up if the surface is hotter than the bed. However, the packets are frequently replaced by new packets at bed

temperature, resulting in a maintained high temperature difference between the bed particles and the surface. When theoretically determining the bed-to-tube heat transfer coefficient, convection from both gas and particles as well as radiation should be accounted for. It should however be mentioned that for small particle sizes (<1 mm) gas convection can generally be neglected [48].

Although FBHEs have been used in high temperature applications (i.e. >400˚C) there are few experimental studies to estimate the bed-to-tube heat transfer coefficient at high bed temperatures. Most of the research on heat transfer from bed to an immersed surface has recently been reviewed by Leckner et al. [45]. Despite the research efforts to provide predictive models for the bed-to-tube surface heat transfer, it is still difficult to make accurate predictive models [45]. In addition, some of the most well-known correlations to predict the heat transfer coefficient to a horizontal tube [48-53] are based on empirical correlations that have been determined at temperatures below 400°C, meaning that the correlations only include convective heat transfer. As a result, extrapolation is required when predicting the bed-to-heat transfer at higher temperatures, which makes the accuracy of the correlations questionable even though the predicted radiative heat transfer to the tube can be added to the predicted convective contribution. It should also be mentioned that most of the previous work has been done with quite large bed particles which may not be the most suitable particle size for CFB/FBHE applications. Silica sand has been used in most of these studies and to verify that the bed-to-tube heat transfer can be estimated also for other bed materials, additional experimental work is required. Another aspect which needs additional attention is the impact of the fluidizing gas. When using existing heat transfer correlations, it can be observed that changing from air as fluidizing gas to flue gas or pure steam is predicted to improve heat transfer significantly, but this should be verified through experimental work.

3. Experimental setup

For the experiments presented in this thesis, three different fluidized reactors were used. The same furnace and general infrastructure for feeding gas to the reactor and measure temperature and pressure was used for the first two reactors. The last reactor is part of a semi-commercial scale CFB boiler. All three reactors are described below.

3.1. OCAC reactor

Experiments on OCAC, which are presented in **Paper IV** were performed in a laboratory-scale high temperature steel reactor, see Figure 5. Air is fed as fluidization gas and a hole plate is used to provide a good gas distribution. Based on the risk of bed particles falling through the distribution plate a gas flow is always maintained through the windbox. The air and fuel gas are premixed before entering the windbox of the bubbling fluidized bed (BFB) reactor. Methane and PSA off-gas were the two fuels tested in the reactor system. The composition of the PSA off-gas used in the experiment was 15 vol-% CH_4, 25 vol-% H_2, 15 vol-% CO and 45 vol-% CO_2. The gas flow to the reactor was set to achieve a superficial gas velocity of 0.2 m/s. An air-cooled cooling coil is located in the windbox to reduce the risk of fuel ignition prior to the actual combustion chamber.

The gas exhaust leaving the BFB is fed to a ventilated hood, where it cools down. The reactor is placed in an electrically heated furnace with three heating zones which can be controlled separately, and where a target temperature can be specified for each zone. The temperature is measured in the windbox as well as at 8 vertical positions, MP1-MP8, both in the bed and in the freeboard, by means of thermocouples. The tubes where the thermocouples are introduced are also used to measure the pressure, by means of pressure transducers. At similar heights on the opposite side, corresponding to the same measurement point named MP1-MP8, gas can be extracted from the reactor. The locations of each measurement point (MP) is presented in Table 1.

***Table 1**: Measurement point (MP) positions in relation to the distributor plate.*

Position	Vertical position [cm]
H_8 (MP8)	79.65
H_7 (MP7)	63.65
H_6 (MP6)	47.65
H_5 (MP5)	31.65
H_4 (MP4)	15.65
Targeted H_{bed}	13.65 to 15.65
H_3 (MP3)	13.65
H_2 (MP2)	8.88
H_1 (MP1)	3.65
H_0 (MP0, in windbox)	-4.00

Gas sampling tubes in stainless steel (316L) with a porous cone in the same material welded to the ends of the tubes (10 mm OD & 6 mm ID) are used to extract gas while preventing bed material from entering the gas sampling tube. Jacketed tubing is used on this side to make it possible to move the tube over the cross section with teflon ferrules in the tube fittings. MP0 represents the measurement point in the windbox where only temperature and pressure measurements are conducted.

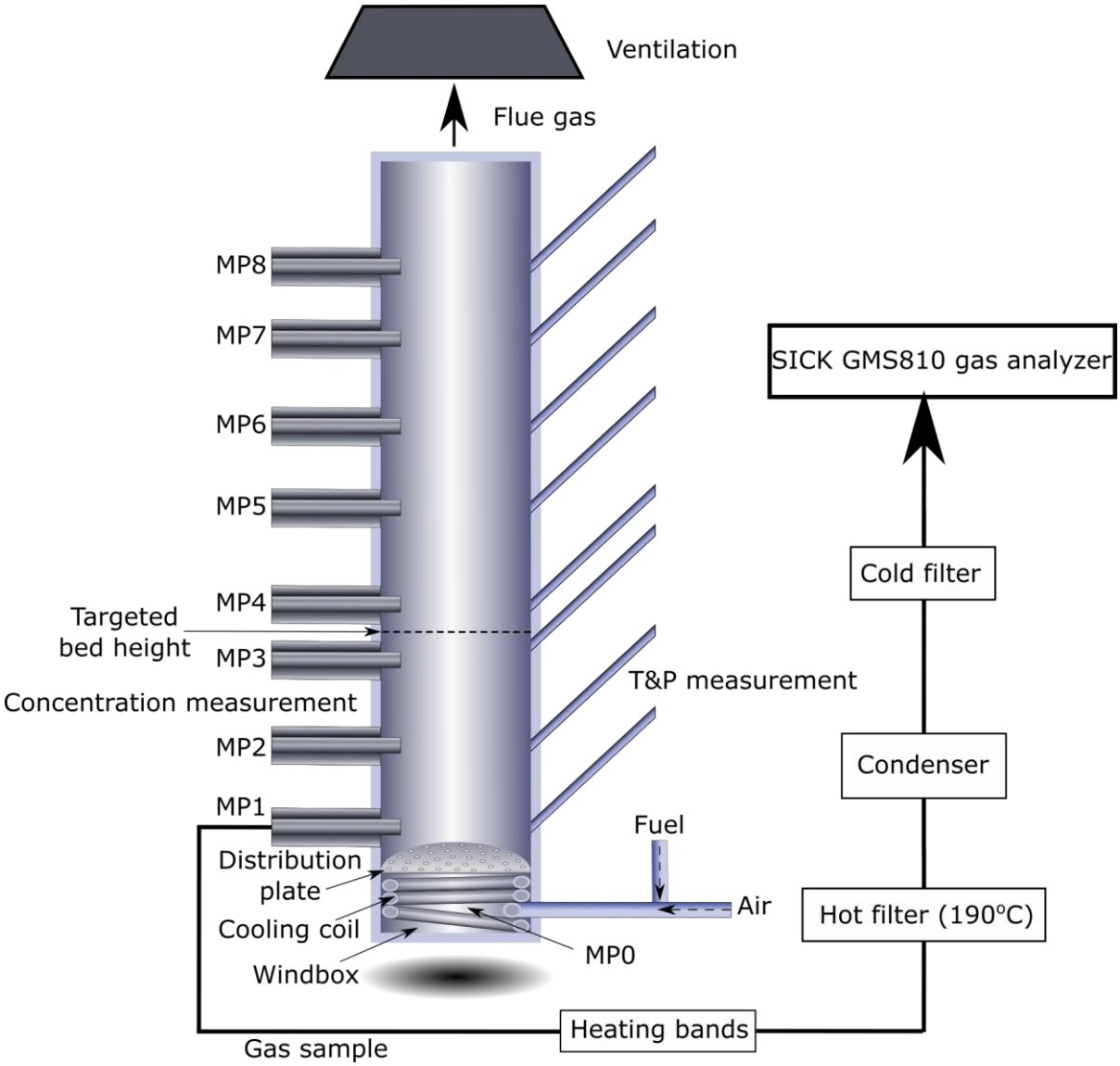

Figure 5*: Schematic illustration of the BFB reactor system with gas sampling tubes to the left and the inclined tubes for the pressure transducers and thermocouples to the right, each corresponding to a certain measurement point, from MP0 in the windbox to MP8 at the top of the freeboard.*

During gas sampling, a heated line is attached to the measurement point (MP1-MP8). The heated line is kept at a temperature of 190˚C to avoid condensation in the extracted gas stream. The sampled gases pass through a hot filter operating at the same temperature as the heated line. The wet gas is dried in a condenser followed by a cold filter before it enters the gas analyser. Nondispersive infrared sensors, NDIR, are used to measure the concentration of CO, CO_2 and

CH_4. O_2 is measured with a paramagnetic sensor and H_2 is detected using measurements based on thermal conductivity. All measurements are made online with one datapoint retrieved every second.

Equal volumes of bed materials were used in the experiments, meaning that the bed mass used was based on bulk density measurements prior to the experiments. The target was to have the bed height H_{bed}, between measurement points MP3 and MP4. Based on the measured gauge pressure at MP3, P_3, the bed height was therefore estimated according to Eq.(5). H_3 is the vertical position of MP3 above the distribution plate. The air density (ρ_g) is assumed to be negligible compared to the particle density (ρ_p) and the voidage of the fixed bed (ε_{fixed}) is assumed to be 0.4, whereas the voidage in the bubbling bed (ε_{BFB}) is assumed to be 0.6.

$$H_{bed} = H_3 + \frac{P_3}{9.81(\rho_p - \rho_g)(1 - \varepsilon_{BFB})} \quad (5)$$

The particle density was estimated based on the measured bulk density of the bed materials (ρ_b) according to Eq.(6).

$$\rho_p = \frac{\rho_b}{1 - \varepsilon_{fixed}} \quad (6)$$

The bulk density was estimated by measuring the mass poured into a known volume according to the ISO standard 3923-1:2008. The minimum fluidization velocity u_{mf} and the terminal velocity u_t presented in Table 2 are calculated for the particles fluidized in air at 750˚C. The thermal input indicated in the same table is estimated for the case with a superficial gas velocity of 0.2 m/s, an air-to-fuel ratio of 1.05 and a bed temperature of 750˚C.

***Table 2**: Bed material characteristics and bed inventory for the experiments in the OCAC reactor.*

	Sand	Ilmenite	C28
Mean particle diameter (μm)	130	163	149
Bulk density (kg/m^3)	1366	2189	1905
Minimum fluidization velocity u_{mf} (cm/s)	0.54	1.37	1.00
Terminal velocity u_t (cm/s)	42.6	96.4	73.2
Solids inventory (g)	854	1369	1191
Fuel input (kW)	0.82	0.82	0.82
Specific bed mass (kg/kW$_{th}$)	1.05	1.68	1.46

The silica sand used in these experiments was supplied by Sibelco Nordic AB from Baskarp. The Norwegian rock ilmenite supplied by Titania A/S. Ilmenite is a mineral ore rich with titanium-iron oxide that is mined mainly for production of titanium dioxide. Ilmenite concentrate is a commonly used oxygen carrier in chemical-looping combustion systems for CO_2 capture, mainly due to its mechanical durability, non-toxicity and relatively low cost [28]. Ilmenite has also been successfully applied as bed material in fluidized bed boilers, where it has been shown to provide several benefits [54, 55]. C28 was manufactured within the EU-funded INNOCUOUS project where the main reason for the interest in the material was due to high reactivity with both

methane/natural gas [56, 57]. A size interval of 90-212 μm was chosen for both materials, where sieving was used to determine also the particle size distribution and the weighted mean particle diameter.

The sand is a practically inert bed material, with respect to oxygen carrying capacity, whereas the ilmenite and C28 are oxygen carriers. The reaction between methane and the most oxidized state of ilmenite which is pseudobrookite (Fe_2TiO_5) and rutile (TiO_2) can be described according to Eq.(7).

$$\frac{1}{4}CH_4 + Fe_2TiO_5 + TiO_2 \Leftrightarrow 2FeTiO_3 + \frac{1}{4}CO_2 + \frac{1}{2}H_2O \quad \Delta H = 35\ kJ/mol\ O \tag{7}$$

The reoxidation of ilmenite can be described by Eq.(8).

$$2FeTiO_3 + \frac{1}{2}O_2 \Leftrightarrow Fe_2TiO_5 + TiO_2 \quad \Delta H = -235\ kJ/mol\ O \tag{8}$$

It should be noted that other reactions can occur as well, such as redox reactions with magnetite (Fe_3O_4) and hematite (Fe_2O_3).

3.2. Lab-scale FBHE reactor

The reactor used in the heat transfer experiments was made from the same material and had the same overall dimensions as the OCAC reactor. The reactor is also operated as a bubbling fluidized bed, the main difference being the presence of a single horizontal tube made of Inconel alloy 600, with an outside diameter of 6 mm which is located in the lower part of the reactor. The unit can therefore be seen as a fluidized bed heat exchanger (FBHE). The tube is placed 7.5 cm above the distribution plate which was welded to the outside wall of the reactor. The distribution plate was similar to the one used for the OCAC reactor but with slightly smaller holes. Water flows inside the horizontal tube from a tap. The water flow rate is controlled with a valve, and to measure the flow rate with high accuracy a scale is placed at the outlet. Pressure is measured at 5 different measurement points using pressure transducers. An outline of the reactor system can be seen in Figure 6.

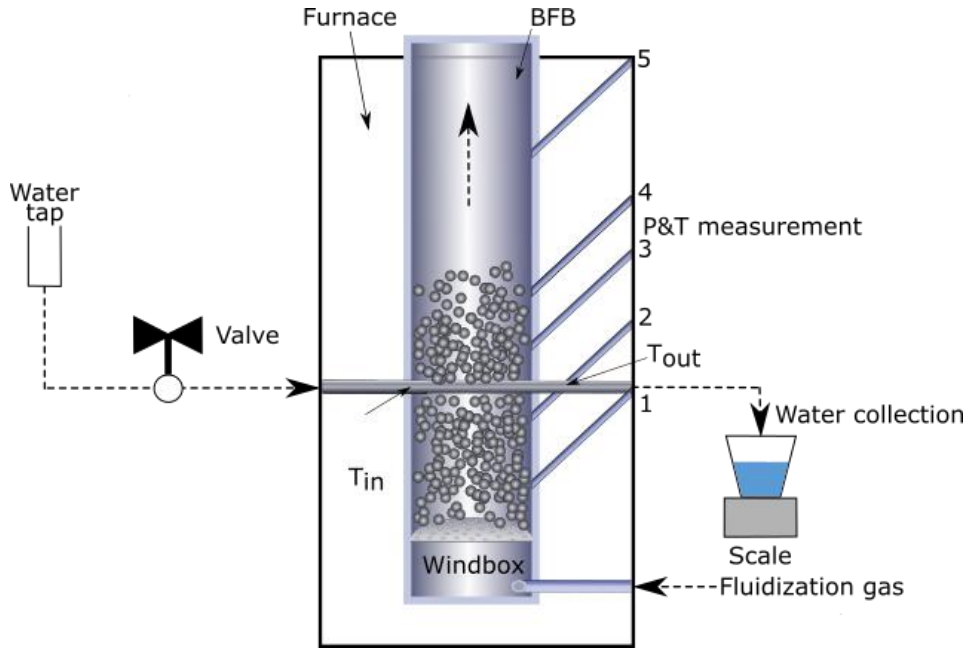

***Figure 6**: Schematic illustration of the BFB system with inclined tubes to the right for the pressure transducers and thermocouples indicating the different measurement points (1 to 5).*

The temperature measured at measurement point 2 was chosen to be used as the estimated bed temperature since it was considered to be at suitable distance from the water tube to represent the temperature of the bed. The bed temperature is used in the calculations of superficial gas velocity as well as the heat transfer coefficient. Thermocouples were also installed at measurement point 1, 3 and 4. The temperature in the water tube was measured at the entrance point and the exit point of the BFB reactor, where the thermocouples were placed in the centre of the water tube.

The water tube at the outlet had to be bent around one of the inclined tubes to fit it inside the furnace, with the result that the thermocouple used to measure the outlet temperature of the water was placed approximately 2 cm from the inside BFB reactor wall. Based on an experiment in which the position at the water inlet to the BFB reactor was varied, it was concluded that this had negligible impact on the measured water temperature at the outlet.

Thermocouples, type K, tolerance class 1, were used. The thermocouples were from the same batch, so the measured temperature should differ no more than 0.1°C between them. The thermocouples have a common reference point and are connected to a NI 9213 measurement module where the measurement is done in high-resolution mode with a measurement accuracy of <0.02°C.

Three different bed materials were used in this work. Equal volumes of bed material were used in all experiments, corresponding to a fixed bed height of 17 cm based on the measured bulk density. The bulk density was estimated using the same approach as for the OCAC reactor tests. The main characteristics of the fresh bed materials before adding them to the unit are presented in Table 3.

***Table 3**: Key characteristics of the bed material batches.*

Bed material	Size range based on sieving [µm]	d_p [µm]	ρ_b [kg/m^3]	u_{mf} [m/s]	u_t [m/s]
Sand	90-212	129	1434	0.006	0.44
Ilmenite	90-212	167	2165	0.015	1.04
Ilmenite	250-355	280	2071	0.040	2.39
LD slag	90-150	123	1471	0.006	0.41
LD slag	150-300	199	1535	0.016	1.03
LD slag	300-355	327	1566	0.042	2.42

All materials were heat treated with air for at least 1 hour in the reactor system prior to the start of the experiments at 950˚C, to ensure that steady state properties of the bed materials were reached. Sibelco Nordic AB supplied the silica sand from Baskarp, the most important sand source in Sweden. Silica sand is the most commonly used bed material in fluidized bed combustion of biomass and waste fuels and also the material which has been most frequently used in studies on heat transfer in fluidized beds. Titania A/S supplied the ilmenite which is physically beneficiated Norwegian rock ilmenite. Based on the possible use of ilmenite in fluidized bed processes it is motivated to evaluate the heat transfer when using this bed material.

The material denoted as LD slag in this article is ground steel converter slag from the Linz-Donawitz production process. The material was provided by SSAB Merox AB. LD slag consists mainly of oxides of Ca, Mg, Fe, Si and Mn. Like ilmenite it is suitable as oxygen carrier in chemical-looping combustion [58, 59]. Large quantities of LD slag are generated but there is currently limited demand in many countries. Hence, due to good availability and potentially very low cost, the material could be suitable for large-scale operation in fluidized bed units, as has been shown recently [41]. Despite the possible uses of ilmenite and LD slag, no previous studies on bed-to-tube heat transfer coefficient in a FBHE using these materials were found which was an additional motivation. Both ilmenite and LD slag could be relevant bed materials in the processes presented in **Papers I-III**.

3.3. Semi-commercial CFB boiler

The experimental work in **Paper VI** was carried out in a 12 MW_{th} CFB boiler interconnected with a 2-4 MW_{th} bubbling bed gasifier located on the campus of Chalmers University of Technology in Gothenburg, Sweden. The boiler is operating continuously during the colder part of the year, November to April, with a fuel load of approximately 5-6 MW_{th} to supply heat for the district heating network. The fuel which was used during the campaign was wood chips.

The most important components of the plant are observed in Figure 7.

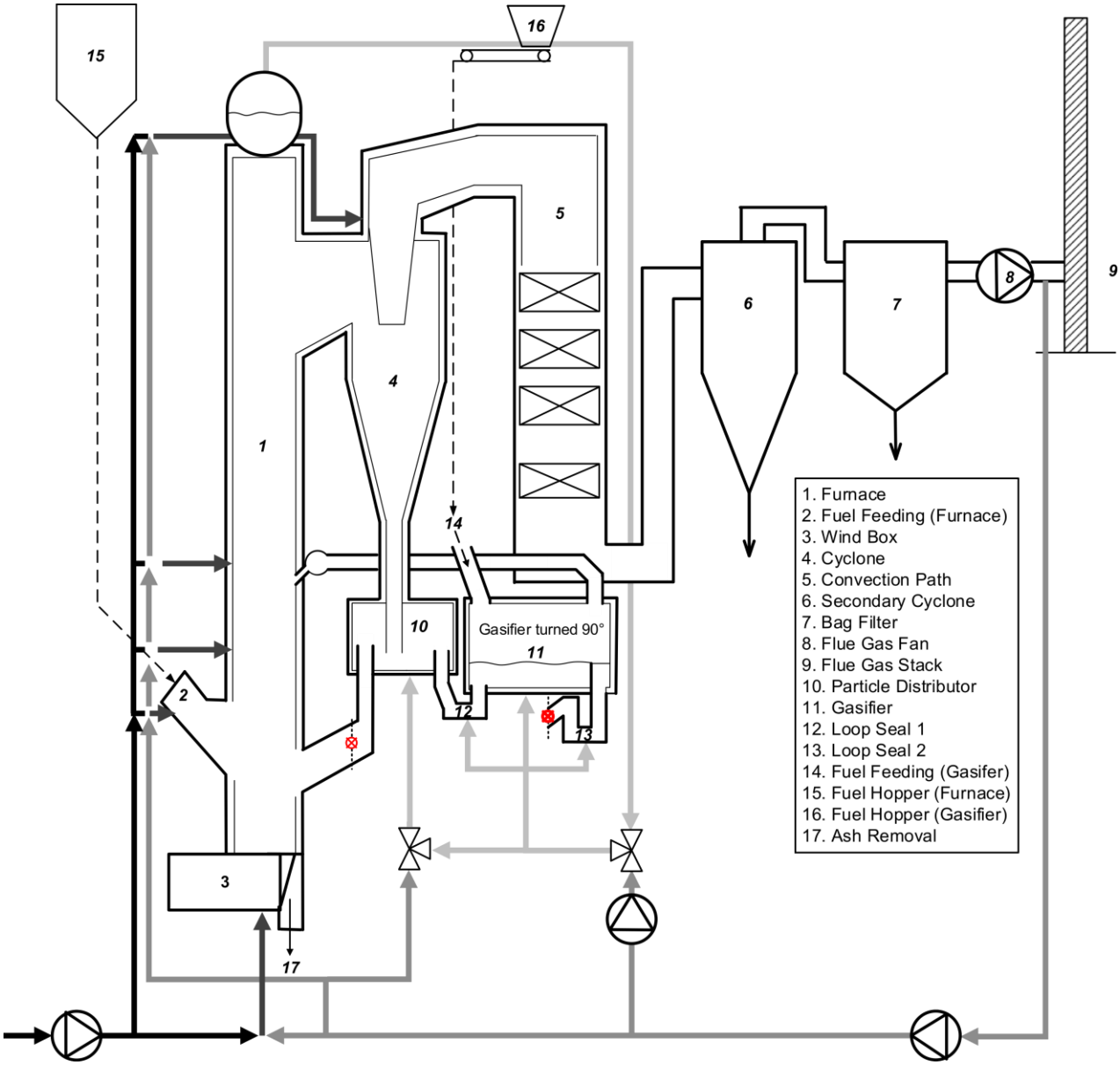

***Figure 7**: Schematic description of the dual fluidized bed boiler/gasifier system at Chalmers University of Technology.*

The fuel is top-fed to the bed through a fuel chute (2). The flue gas is, together with entrained bed material, transported to the water-cooled cyclone (4). In the cyclone, bed material is separated from the flue gas and falls into the particle distributor (10). The bed material can from that point be circulated back to the furnace or transported to the gasifier (11) by passing through loop seal 1 (12). An overflow exit then connects the gasifier with loop seal 2 (13) which leads the particles back to the furnace. A specially designed heat transfer probe was inserted from above into loop seal 1 through a flange. The probe consists of a vertical U-tube in stainless steel through which water is flowing at a high velocity. The U-tube can be oriented both in parallel and perpendicularly to the particle flow. The heat transfer coefficient from bed to tube can be assessed from temperature measurements with thermocouples at a targeted height on the water side as well as inside the process in the particle distributor and the gasifier. Bed material was sampled from the center of the loop seal during operation.

The gas velocity can be varied as well as the fluidization gas of the loop seal where air, flue gas and steam are available. In addition, the circulation rate of bed material passing through the loop seal could be varied mainly by changing the gas velocity at the bottom of the furnace. The gas composition, temperature and pressure are monitored and logged continuously at various points in the reactor system during the experiments.

Silica sand and ilmenite were the two bed materials used in **Paper VI**. The sand was provided by Sibelco Nordic AB (Baskarp B28) with mainly SiO_2. The ilmenite was rock ilmenite concentrate from Titania A/S in Norway. The mean particle size of the material was estimated based on sieving, see Table 4. Bulk densities were determined using the same method presented in **Papers IV & V**. In this experiment both fresh and used bed samples were evaluated with respect to particle size and bed density where the used samples were based on samples collected from loop seal 1 during operation. The campaign with ilmenite took place the 13-14th of December 2018 and the sand campaign the 10-11th of January 2019.

***Table 4**: Estimated weighted mean particle diameter for fresh and used bed materials.*

	Ilmenite fresh	Ilmenite used	Ilmenite used	Sand fresh	Sand fresh	Sand used
Sample time	-	2018-12-13	2018-12-14	-	-	2019-01-11
Sieved by	Manufacturer	Author	Author	Manufacturer	Author	Author
d_p [µm]	198	208	206	265	270	425
ρ_b [kg/m^3]	2343	2034	2006	1444		1275

In Table 4 a clear difference in size can be observed between the fresh material and the used material where the fresh material is smaller. This could be attributed to adsorption of ash elements and sintering of particles. In the case of ilmenite it could also be caused by the fact that fresh ilmenite particles tend to increase in size and reduce its bulk density when going through some redox cycles (oxidized and reduced in contact with fuel and oxygen) [60]. The difference in bed particle size increase during operation between sand and ilmenite this considered to be caused by sand having a higher agglomeration tendency due to risk of formation of alkali silicates [61]. These compounds cause the particles to adhere together and cause agglomeration at high temperature. This difference between sand and ilmenite where sand has a higher agglomeration tendency has been confirmed in separate agglomeration tests presented in **Paper VI**.

In order to reduce the risk of bed agglomeration, the regeneration rate of sand was kept at 250-300 kg/day during the campaign. Each day fresh sand was fed into the boiler and the average residence time of sand was estimated to around 340 h. The chosen regeneration rate was based on previous operation with sand with the same fuel. The reason for a higher agglomeration tendency in these experiments, compared to previous operations with sand as bed material was most likely that the furnace temperature was higher in these experiments.

4. Methodology

This thesis includes: 1) thermodynamic evaluation of three processes where FBHEs are integrated in SMR plants and comparison with the conventional SMR plant; 2) economic evaluation of these processes and comparison with conventional SMR; 3) experimental investigation of OCAC using methane and PSA syngas as fuel with silica sand, ilmenite and C28 (synthetic particles of calcium manganate) as bed material; and 4) experimental investigation of bed-to-tube heat transfer to a tube immersed in a bubbling fluidized bed. The method used in the first two parts are to a great extent based on process simulation in Aspen Plus, while the last two parts involves experiments at lab-scale and semi-commercial scale.

4.1. Thermodynamic evaluation

The possibility to produce hydrogen by integration of steam reforming with OCAC and CLC (denoted by the letters O and C respectively) is evaluated in **Paper I**. A thermodynamic analysis is conducted in these papers to evaluate three alternative process configurations including fluidized bed heat exchangers in relation to a reference SMR plant with a gas-fired furnace as reformer furnace. Two of the proposed cases include the use of methane (M) as supplementary fuel while one of the CLC systems uses biomass (B). The three alternative outlines are illustrated in Figure 8.

Case OM consists of a single fluidized bed heat exchanger which is used to heat the reformer tubes while case CM has the reformer tubes placed in the fuel reactor as part of a CLC system for CO_2 capture. The fuel reactor is operated as a BFB whereas the air reactor is operating as a CFB which provides circulation of the bed material. Case CB also includes a CLC system, but the reformer tubes are no longer placed in the fuel reactor as a result of the risk of formation of ash melts (slagging) on the reformer tubes as a result of the presence of solid biomass. In **Paper I** the tubes are instead placed in an external FBHE which is interconnected with both air reactor (AR) and fuel reactor (FR). The external FBHE was proposed in **Paper I** based on the target to avoid interaction with potentially corrosive compounds in the biomass. The tubes were not placed in the AR in **Paper I** since it was assumed that this unit should be a CFB to provide circulation.

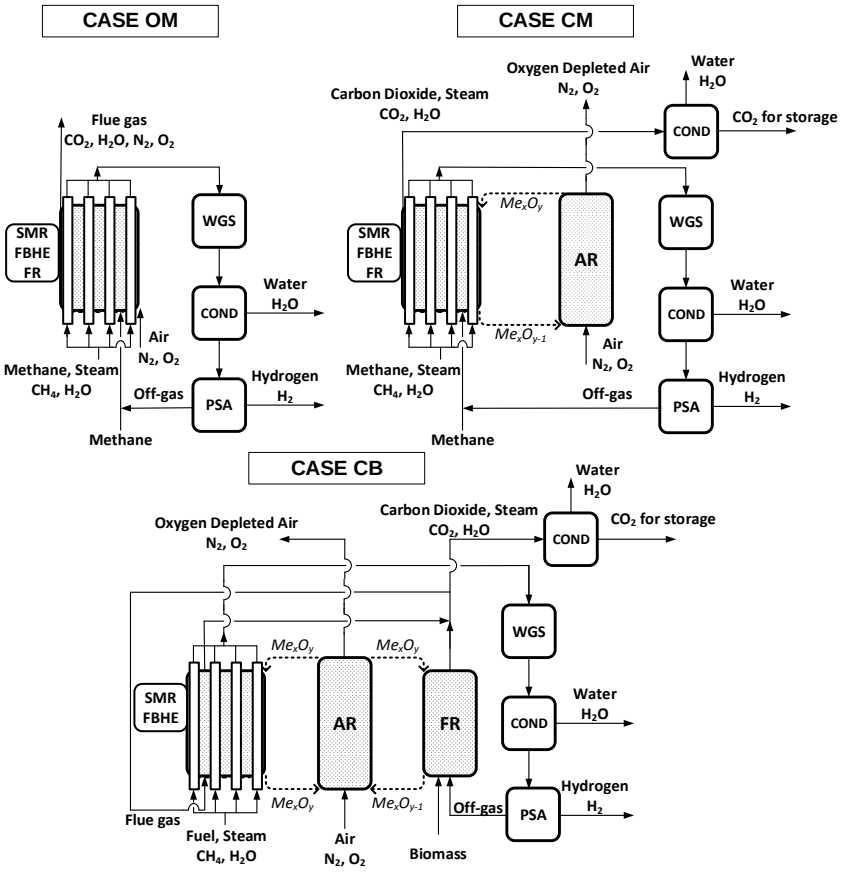

***Figure 8**: Schematic illustration of the three alternative process configurations OM, CM and CB.*

The purpose of the model used in **Paper I** was to identify and estimate the possible benefits of the different processes by estimating the hydrogen production efficiency (named cold gas efficiency in **Paper I**) which is based on the required fuel input per hydrogen produced. An additional purpose was to estimate the decrease in waste heat generated in the alternative configurations compared to the conventional process which is presented as case A.

In all cases studied in **Paper I** methane and steam at 25 bar is preheated to 650˚C before reaching the reformer. The syngas produced is leaving the reformer at 850˚C and cooled to 300˚C before it is fed to a low-temperature WGS reactor followed by another cooler to condense the steam. The steam is removed and thereafter the dry stream is fed to a PSA unit to separate the H_2 product stream with 100% purity. The off-gas stream from the PSA is fed to the reformer furnace, to which also supplementary fuel and preheated air at 600˚C is fed. The heat required for the steam reforming is withdrawn from the FBHE unit in case OM, CM and CB or from the gas-fired furnace (GFF) unit in case A. In the CLC-configurations, it is assumed that there is no temperature difference between the fluidized bed units. One of the key differences between case CB and the other cases in **Paper I** is that a higher hydrogen yield is achieved in the reformer which is motivated by the possibility to reduce the fossil input per hydrogen produced. This is done by using a higher steam-to-carbon ratio (5 instead of 3) and a higher outlet temperature from the reformer (900˚C instead of 850˚C).

In order to compare the four plant configurations, it was decided that all four plants should have the same external tube surface area in **Paper I**. Several assumptions relating to the heat transfer in the conventional furnace and in the targeted fluidized bed heat exchangers are used to estimate the

required flue gas temperatures in the respective processes. It should be accentuated that these estimations to compare the reformer furnace for the different cases in **Paper I** should be seen as first estimations to visualize the potential of the proposed FBHE configuration. A better estimation can be done by presenting a possible FBHE design of suitable size and making more in depth calculations of the heat transfer in the reformer (see **Paper II**). For the pressure drop calculations the FBHE units were assumed to have a bed height of 5 m, bed voidage of 0.5 and a bed particle density of 2800 kg/m^3 and a distribution plate which provides a pressure drop corresponding to 30% of the pressure drop over the bed. This resulted in a pressure drop of 0.89 bar over the FBHE units. The pressure drop over the GFF in case A is neglected in this case. The other key assumptions for the four cases are presented in **Paper I**.

Models for the cases described in **Paper I** are included in an Aspen Plus simulation where a molar flow rate of 1 mol/s methane in the feed stream was used in all cases studied. The biomass supplied to case CB which is simulated as a typical gas composition of gasified biomass, has a Lower Heating Value (LHV) of 15 kJ/kg and consists of CH_4, CO, H_2 and C_3H_6. The air-to-fuel ratio for each case was calculated based on the known molar flows of the combustible products in the furnace. Additional assumptions included in the Aspen Plus model are presented in **Paper I**.

The thermodynamic evaluation presented in **Paper I** should be seen as a principal description of the concepts and identification of possible process configurations including both a single fluidized bed system and dual fluidized bed systems for CO_2 capture. In **Paper II** a much more complete flowsheet is provided for a reference SMR plant for hydrogen production, called case A also in this paper, and the single FBHE system is also presented as case OM in **Paper II**. The flowsheet of case OM in **Paper II** can be observed in Figure 9. Another difference between **Paper I** and **Papers II-III** is that NG is used as supplementary fuel instead of methane which is used in **Paper I**.

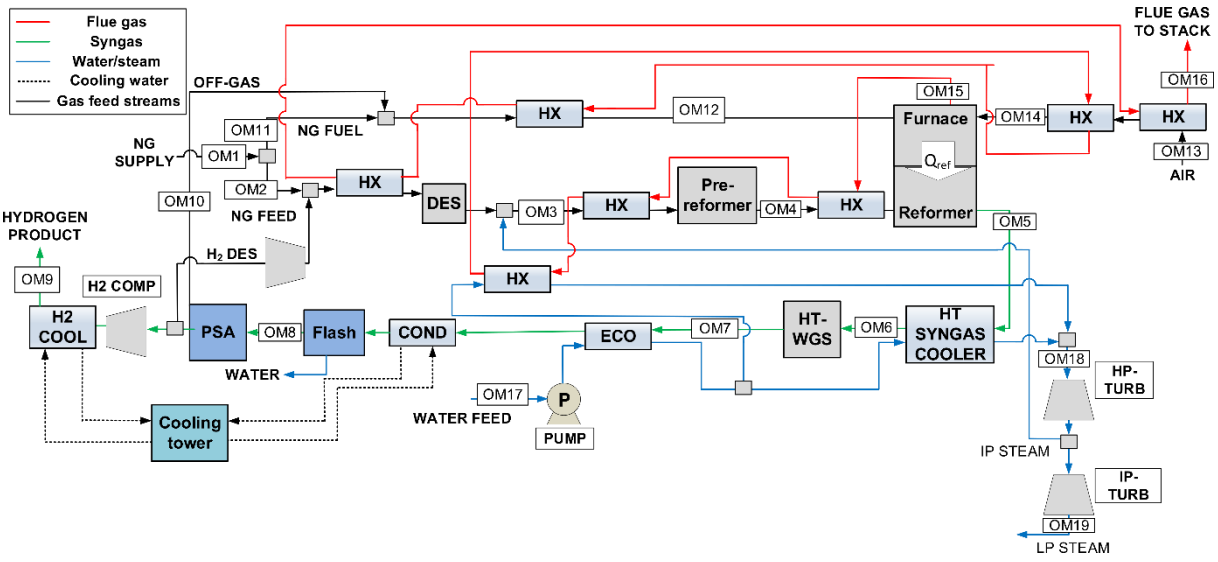

***Figure 9**: Schematic illustration of case OM where the reformer is integrated with a FBHE unit with OCAC. The scheme includes thermal integration with a steam cycle.*

In **Paper III** a more detailed flowsheet is established for the cases where the reference SMR plant is integrated with chemical-looping combustion. The flowsheet for the process where biomass is considered as supplementary fuel instead of natural gas is presented in Figure 10.

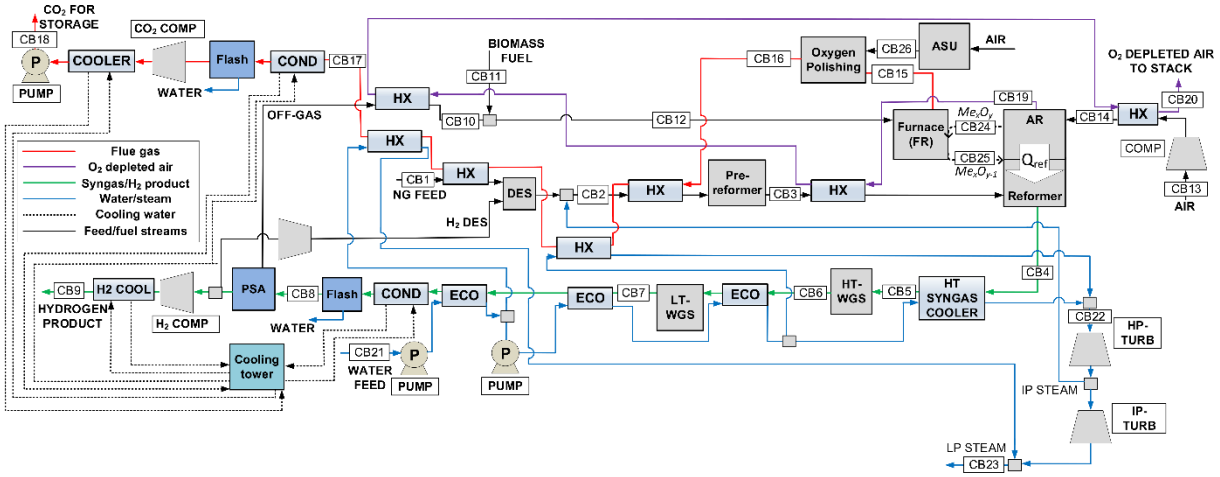

***Figure 10**: Schematic illustration of case CB where the reformer is integrated with a FBHE unit in the AR of a CLC system. The scheme includes thermal integration with the steam cycle.*

The plants presented in **Papers II-III** are also dimensioned to provide a target production rate of hydrogen suitable for a large-scale production plant. The plants also include thermal integration with preheating of reactants and a heat recovery steam generator system, which produces intermediate pressure used in the steam reforming directly, as well as high pressure steam. A high pressure steam turbine and an intermediate pressure steam turbine are included in the model and the excess heat generation in form of low pressure steam is also evaluated. The model of the hydrogen production plant in **Papers II-III** also include a more in-depth analysis of a possible FBHE design, choice of oxygen carrier and an evaluation of suitable operating parameters based on both hydrogen production efficiency and levelized hydrogen production cost.

Numerous possible performance indicators are possible for the processes compared in **Papers II-III**. The energy stored in the NG fed to the plant can be converted into hydrogen, electricity and heat. The possible use of electricity/heat can be related to the energy required to produce this electricity/heat in a state-of-the-art industrial plant. The approach presented by Martinez et al. [62] is used to compare the performance of the processes. The parameters used are summarized in Table 5 with Eq.(9)-(16).

***Table 5**: Parameters used in thermodynamic evaluation of the plants.*

Hydrogen production efficiency (%)	$\eta_{H_2} = \frac{\dot{m}_{H_2} \cdot LHV_{H2}}{\dot{m}_{biomass} \cdot LHV_{biomass} + \dot{m}_{NG,tot} \cdot LHV_{NG}}$	(9)
Equivalent flow of CH_4 (mol/s)	$\dot{M}_{CH4,eq} = \dot{M}_{CH4} + \frac{7}{4}\dot{M}_{C2H6} + \frac{5}{2}\dot{M}_{C3H8} + \frac{13}{4}\dot{M}_{C4H10}$	(10)
Equivalent flow of NG (kg/s)	$\dot{m}_{NG,eq} = \dot{m}_{NG,feed} + \dot{m}_{NG,eq,bio} - \frac{Q_{th}}{\eta_{th,ref} \cdot LHV_{NG}} - \frac{W_{el}}{\eta_{el,ref} \cdot LHV_{NG}}$	(11)
Equivalent flow of biomass (kg/s)	$\dot{m}_{NG,eq,bio} = \frac{\dot{m}_{biomass} \cdot LHV_{biomass}}{LHV_{NG}}$	(12)
Efficiencies reference plants	$\eta_{th,ref} = 0.9 \;\; \eta_{el,ref} = 0.583$	
Heat delivered from steam export	$Q_{th} = \dot{m}_{steam,exp} \cdot (h_{sat,vap,6bar} - h_{sat,liq,6bar})$	(13)
Hydrogen yield (%)	$Y_{H2} = \frac{\dot{M}_{H2}}{\dot{M}_{CH4,eq}}$	(14)
Equivalent hydrogen production efficiency (%)	$\eta_{H_{2,eq}} = \frac{\dot{m}_{H_2} \cdot LHV_{H_2}}{\dot{m}_{NG,eq} \cdot LHV_{NG}}$	(15)
Equivalent hydrogen production efficiency (assuming all LP steam converted to electricity in a LP steam turbine) (%)	$\eta'_{eq,H_2} = \frac{\dot{m}_{H_2} \cdot LHV_{H_2}}{\dot{m}_{NG,tot} \cdot LHV_{NG} - \frac{W'_{el}}{\eta_{el,ref}}}$	(16)
Conversion factor LP steam turbine	Electricity production LP steam turbine = $0.1Q_{th}$	
CO_2 specific emissions ($g_{CO_2}/MJ_{H2\ produced}$)	$E_{CO_2} = \frac{\dot{m}_{CO_{2,emitted}}}{\dot{m}_{H2,prod} \cdot LHV_{H2}}$	(17)

W_{el} represents the net electricity production of the plant and W'_{el} is the sum of W_{el} and the electricity that could be produced by expanding the available LP steam in a LP steam turbine.

4.2. Economic evaluation

The model of the hydrogen production plant in Aspen Plus is used as a basis for the economic assessment of the conventional SMR plant and the plant including a single FBHE integrated in a SMR plant. The economic analysis carried out in **Papers II-III** includes both capital and operational costs to estimate a levelized production cost of hydrogen production (LCOH). A Bottom-Up Approach (BUA) is used where the cost of the most important components is estimated based on the cost of reference components (C_o) with a similar function and the reference capacity S_o and scaled based on targeted capacity (S), see Eq.(18). The cost of the reference component is estimated for year x. The scale factor is represented as n and z is the number of required units of the reference component.

$$C = z \cdot C_o\left(\frac{S}{zS_o}\right)^n \cdot \frac{CEPCI_{2015}}{CEPCI_{year\ x}} \quad (18)$$

The Chemical Engineering Plant Cost Index (CEPCI) is used to relate costs of process equipment for a certain year to the base year (2015). A Capital Charge Factor (CCF) is used to annualize the total cost to construct the operational plant.

The equipment cost of the conventional gas-fired furnace (GFF) is estimated based on the cost estimation provided by Turton et al. [63]. The cost of a fluidized bed reactor is estimated based on cost estimation of a fuel reactor design provided by plant manufacturer Bertsch within the EU-funded SUCCESS project [64], with the cost of the reformer tubes added on top of it. The cost to replace the high alloy steel reformer tubes are based on the price indication provided by Roberts and Brightling [65] of 20000 US$/reformer tube. The reformer tubes in the conventional gas-fired furnace are assumed to have a life time of 50 000 hours in the conventional plant, but twice as long in the FBHE, assuming the same tube material to be used.

LCOH is the main performance indicator from an economic point of view in **Papers II-III** but **Paper III** also includes an estimation of the cost of CO_2 avoidance (CCA) which is a measure of the added cost to capture CO_2 for a certain plant compared to a reference plant with no capture (see Eq.(19)).

$$CCA = \frac{LCOH_i - LCOH_{case\ A}}{E_{CO_2,case\ A} - E_{CO_2,i}} \tag{19}$$

4.3. Experimental investigation of OCAC in BFB

The OCAC experiments are carried out in the OCAC reactor described in chapter 3. The pressure and temperature were measured continuously for all measurement positions and the gas composition was measured continuously for one vertical position at a time. The targeted fuel flow was added to the system once the furnace had reached its setpoint value in the temperature range 600-900˚C with methane as fuel and 600-800˚C with PSA off-as as fuel which was based on that PSA off-gas is more easily converted in the reactor. Measurement data was then extracted once steady state operation was observed with respect to measured pressure, temperature and gas concentrations.

When the gas sampling probe is placed at a certain height the gas concentration at that point is measured, as well as the average temperature and pressure at all measurement points. The superficial gas velocity was kept at 0.2 m/s based on the set furnace temperature and the volumetric flow of air fed to the system. The air-to-fuel ratio (AFR) was set to 1.05. The AFR is defined as the ratio of the volumetric flow rate of air fed to the fluidized bed to the volumetric flow rate corresponding to stoichiometric combustion of methane. The stoichiometric amount of air is based on the amount of oxygen needed to convert the fuel fed to the reactor, e.g. according to Eq.(20) for methane:

$$CH_4 + 2\,O_2 \rightarrow CO_2 + 2\,H_2O \qquad \Delta H_{298°C} = -802.3\ kJ/mol \tag{20}$$

If CO rather than CO_2 is detected it indicates that the combustion is incomplete, and the amount of CO detected can also be related to the inlet concentration of CH_4 since it is the only source of carbon fed to the system.

With methane as fuel, CH_4, CO and CO_2 were used to evaluate the combustion efficiency and with PSA off-gas as fuel the measurement of H_2 was also evaluated. Since the setup only measures dry

gases due to steam condensation prior to the analyser, the steam content in the gas was not quantified.

4.4. Experimental investigation of bed-to-tube surface heat transfer in FBHE

The bed-to-heat transfer was evaluated experimentally in **Papers V & VI**. The same basic principle was used, where the water temperature at the inlet and outlet from the reactor, as well as the water flow rate and the bed temperature were measured. The heat transfer coefficient on the inside of the tube was determined using established correlations for liquid flow in tubes. The liquid was water with a temperature well below 100°C in both experiments. The gas flow rate to the fluidized bed was adjusted based on the bed temperature, to obtain the targeted superficial gas velocity.

The heat delivered to the water tube was estimated based on the temperature difference between inlet and outlet and the heat capacity of water. The overall heat transfer coefficient (U_o) could then be estimated based on the known tube surface area and the logarithmic mean temperature difference between the bed and the water. The temperature of the inside tube wall was estimated based on known heat load, inside heat transfer coefficient (see Eq.(21)) and the inside area of the tube.

$$T_{s,i} = \frac{Q}{h_i A_i} + T_{water} \tag{21}$$

The heat transfer coefficient through the wall and the temperature on the outside of the tube could then be estimated by using Eq.(22) and (23) through iterative calculations. The thermal conductivity of the tube wall is dependent on the wall temperature and it was estimated based on an average of the estimated temperature on the inside and outside tube surface.

$$h_w = \frac{2k_w}{d_o \ln\left(d_o/d_i\right)} \tag{22}$$

$$T_{s,o} = \frac{Q}{h_w A_o} + T_{s,i} \tag{23}$$

The estimated surface temperature on the outside of the water tube was also used to estimate the radiative heat transfer from bed to tube. The bed-to-tube heat transfer coefficient on the outside of the tube, h_o, including both radiative heat transfer and convective heat transfer was estimated using Eq.(24) [66].

$$h_o = \frac{1}{\frac{1}{U_o} - \frac{d_o \ln(d_o/d_i)}{2k_w} - \frac{d_o}{d_i h_i}} \tag{24}$$

The experimentally determined bed-to-tube surface heat transfer coefficient was compared with heat transfer correlations, which can be used for prediction for example in process modelling. These correlations have been determined using experiments performed by different researchers using a wide range of materials, equipment sizes and reactor configurations. Some of the most

well-known correlations describing the bed-to-tube heat transfer coefficient were evaluated in **Paper V** where these are presented in more depth [67].

All the heat transfer correlations presented from literature have been established using a bed temperature below 400˚C and most of the correlations have used an electric heating rod to heat the fluidized bed which is opposite to the principle to use the FBHE as a heat source as presented in **Papers I-III** for example. Based on the target of this study, which is to operate a BFB at high temperature, it is therefore important to verify if the heat transfer correlations presented could be used also for higher bed temperatures. This can be achieved by comparing the experimentally determined heat transfer to the tube with the heat transfer predicted with heat transfer correlations.

In order to compare the estimated values for h_o, the radiative heat transfer coefficient was estimated (see Eq.(25)) where the emissivity of the bed, e_b, is estimated based on assumed particle emissivity ($e_b=0.5(1+e_p)$). The particle emissivity [66] and the emissivity of the tube wall surface [68], e_s, were both assumed to be assumed 0.9.

$$h_{rad} = \frac{\sigma\left((T_b + 273.15)^4 - (T_{s,o} + 273.15)^4\right)}{\left(\frac{1}{e_b} + \frac{1}{e_s} - 1\right)\left(T_b - T_{s,o}\right)} \tag{25}$$

Since the contribution from radiative and convective heat transfer to the tube surface are additive, the convective contribution can be estimated as h_o - h_{rad}.

The general approach in both papers was to adjust one parameter at a time, while keeping the others constant. In the base case for **Paper V** the bed temperature was kept at 825˚C, the superficial gas velocity was 0.15 m/s. The water flow rate was 20 ml/s.

The methodology for **Papers V-VI** is quite similar. However, in the semi-industrial scale heat transfer experiment presented in **Paper VI**, it was more difficult to keep all but one parameter constant at a time. The targeted bed temperatures in the loop seal was 800 and 850˚C while it was attempted to have two different circulation rates, one “high” and one “low”. The targeted bed temperature in loop seal 1 is reached mainly by adjusting the fuel input to the boiler. The circulation flow rate is controlled by controlling the gas velocity in the primary zone of the furnace which should control the amount of bed material entrainment to the cyclone. The U-tube was placed in two different positions: parallel and perpendicular orientation in relation to the particle flow. Three different fluidization gases were used in these experiments: air, flue gas and steam. A variation of the gas velocity was attempted within a range which made it possible to maintain circulation through the loop seal.

5. Results and discussion

This chapter presents the key results of this thesis work. The first section presents the evaluation of the proposed processes based on thermodynamics, which is found on **Papers I-III**. The second part includes the economic evaluation which is presented in **Papers II-III**. The third section presents the results of **Paper IV** concerning the experimental investigation of oxygen carrier aided combustion, whereas the fourth section presents the studies of bed-to-tube heat transfer which involves the results of **Papers V-VI**.

5.1 Thermodynamic evaluation

The key objective of **Paper I** was to evaluate basic thermodynamics of plants where FBHEs were used as a heat source for steam reforming. A parameter which was used to evaluate the thermodynamic performance of the plants was the hydrogen production efficiency, presented as cold gas efficiency in **Paper I**. This parameter is the ratio between the heat stored in the H_2 produced in relation to the total thermal input to the plant adding up the feed and supplementary fuel.

The process first proposed, named case OM, includes a single FBHE and is the case which introduces the least new changes in relation to the reference plant. The use of the fluidized bed heat exchanger results in an improved heat transfer to the reformer tube enabling a lower flue gas temperature compared to the conventional reformer furnace. This lowers the supplementary fuel consumption and raises the hydrogen production efficiency from 76.4% to 79.4%, see Table 6. The reduction of the supplementary fuel consumption also leads to a reduction of the CO_2 emissions and the excess heat production is reduced mainly due to a reduced flue gas temperature from the reformer furnace.

***Table 6**: Specific process characteristics for all the studied cases in **Paper I**.*

Case	A	OM	CM	CB	
Hydrogen yield (%)	71.67	71.67	71.67	85.75	Ratio between produced hydrogen and the hydrogen which could be ideally produced from the hydrocarbons in the feed stream
T_{fg} (˚C)	1070	950	950	1000	Reformer furnace flue gas temperature
Supplementary fuel (%)	13.23	8.55	8.95	38.6	Additional fuel fed to the furnace in relation to the amount in feed (% on LHV basis)
η_{H_2} (%)	76.4	79.7	79.4	74.6	Hydrogen production efficiency based on LHV
CO_2 emissions (kg CO_2/m_n^3 H_2)	0.776	0.744	0	-0.391	Emissions of CO_2 for the overall process per m^3 produced H_2 at standard conditions
Change in CO_2 emissions (%)		-4.1	-100	-150.4	Change in CO_2 emissions in relation to the emissions for the conventional plant, case A
Excess heat (kW)	81.5	44.8	47.9	58.3	Excess heat above the pinch point
Thermal input (kW)	908.2	870.7	873.9	1111.5	Thermal input for the plant including feed and supplementary fuel
Share of thermal input (%)	9.0	5.2	5.5	5.2	Relation between excess heat to the thermal input

Case CM is similar to case OM, the main difference being that it has an additional fluidized bed reactor to enable inherent CO_2 capture using chemical-looping combustion. This addition increases the supplementary fuel consumption slightly and lowers the hydrogen production efficiency but with the added benefit of obtaining a plant with net zero emissions of CO_2. The process is still significantly more efficient than the reference plant with a hydrogen production efficiency of 79.4%.

Case CB builds just as case CM on a CLC system, but the operational parameters are different as a result of the use of biomass as supplementary fuel. The target of this process is to obtain a system producing hydrogen while obtaining net negative emissions. To increase the amount of negative emissions, the supplementary fuel consumption of biomass can be increased in relation to the fossil input in the feed stream. By operating at a higher S/C ratio and a higher reformer outlet temperature it is possible to increase the hydrogen yield, i.e. the amount of hydrogen produced per hydrogen which could be ideally produced from the hydrocarbon in the feed stream. The heat duty which must be transferred to the reformer tubes is higher in case CB compared to the other three processes which together with a higher targeted furnace temperature results in a higher supplementary fuel consumption. Although a higher hydrogen yield is reached in the process, the hydrogen production efficiency is reduced and the value is lower than for the conventional plant, case A. The excess heat production is increased compared to case OM and CM but still clearly lower than for the conventional plant when relating it to the total thermal input. The most interesting result from case CB however, is that significant net negative emissions of CO_2 can be obtained from the plant. Both case CM and CB could be highly attractive in a future energy system where significant emissions reductions are required.

All three proposed processes were considered interesting for a more detailed evaluation of the thermodynamics. **Paper II** presents a more detailed thermodynamic evaluation of two large-scale hydrogen production plants including one conventional SMR plant and a plant using a single FBHE. **Paper III** is based on the same framework as presented in Paper II but adds two more processes based on integration of SMR with CLC.

A key design parameter in **Papers II-III** was the flue gas temperature in the reformer furnace for all the evaluated cases and the estimation of this temperature was done using a much more elaborate approach than in **Paper I**. Assuming that the same reformer tube area is used in the reference plant and in the processes based on using the fluidized bed as a heat source, the required flue gas temperature can be reduced significantly since the heat transfer is more efficient. This explains why the required flue gas temperature is the highest in the reference plant both in **Papers I-II**. The result of these calculations is visualized in Figure 11 and shown in Table 7 where the calculated heat transfer coefficients are presented as well as the logarithmic mean temperature difference for case A and OM in **Paper II** and case CM and CB in **Paper III**. The temperature drop at the inlet of the reformer in Figure 11 is connected to the endothermic nature of the SMR reaction.

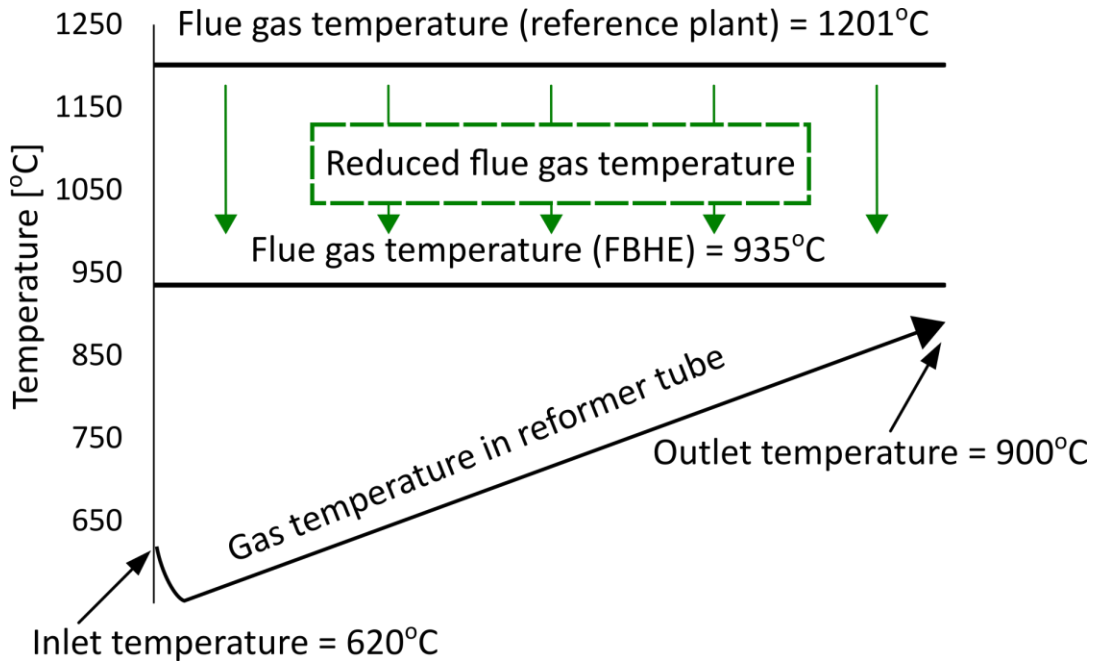

***Figure 11**: Illustration of the temperature profiles used in the model of case A and OM and the temperature of the gas in the reformer in **Paper II**.*

In addition to the mentioned differences in the model of the FBHE unit, the two plants presented in **Paper II** and the two additional plants described in **Paper III** include more components and a more in-depth process configuration. This also includes more details of these plants, as presented in **Papers II-III**, but the most important results from the analysis are displayed in Table 7.

***Table 7**: Key results for the thermodynamic performance of case A and OM in **Paper II** and case CM and CB in **Paper III**.*

		Case A	Case OM	Case CM	Case CB
Heat transfer coefficient inside reformer tube	$W/(m^2K)$	1384	1384	1384	1296
Heat transfer coefficient through tube wall	$W/(m^2K)$	2872	2872	2872	2837
Heat transfer coefficient outside reformer tube	$W/(m^2K)$	138	671	764	665
Overall heat transfer coefficient	$W/(m^2K)$	118	370	396	359
Logarithmic mean temperature difference	˚C	450	144	134	122
Reformer furnace flue gas temperature	˚C	1201	935	929	922
Net electric power	MW_{el}	12.3	2.6	-4.1	-7.3
Steam export (160˚C, 6 bar)	kg/s	18.8	4.1	7.6	9.2
Hydrogen yield after WGS, $Y_{H2,WGS}$	%	78.5	78.5	78.5	93.1
Thermal input NG	MW_{LHV}	423.1	378.9	392.8	298.9
Thermal input biomass	MW_{LHV}				115.4
H_2 production efficiency η_{H_2}	%	70.7	79.0	76.2	72.2
H_2 production efficiency $\eta_{H_{2,eq}}$	%	83.9	82.1	78.4	73.9
H_2 production efficiency η'_{eq,H_2}	%	75.8	80.2	75.4	70.1
CO_2 specific emissions, E_{CO_2}	$g_{CO_2}/MJ_{H2\ produced}$	80.7	72.2	0	-34.1
Total plant CO_2 emissions	Mton CO_2/year	0.69	0.61	0	-0.29

In the comparison between case A and OM it can be observed that the flue gas temperature is significantly lower in case OM and the estimated difference was larger than what was assumed in **Paper I**. The high flue gas temperature in case A is the main reason for excess heat production being significantly higher in case A in relation to case OM, where the assumed steam cycle delivers electricity and heat in excess in form of low-pressure steam at 6 bar. It can be observed in Table 7 that the excess electricity generation and the steam export are significantly higher for case A in relation to case OM. Excess heat generation is common for SMR plants and since the plant is assumed to be located at a refinery it is reasonable to assume that there is limited use of excess heat/electricity. The possibility to export excess electricity and the possibility to use this electricity for additional hydrogen production by electrolysis of water was evaluated as well but the possible economic benefits seem limited. Based on this assumption the hydrogen production efficiency η_{H_2}, which only considers the produced hydrogen as a valuable output, is the most interesting parameter to consider. The hydrogen production efficiency is approximately 12% higher for case OM and the CO_2 emissions are reduced with a similar percentage. Case OM has thus advantages compared to the reference plant both from an economic point of view thanks to the possibility to reduce the fuel consumption and from an environmental point of view by reducing the CO_2 emissions from the process. The only situation where case A presents a higher hydrogen production efficiency is when both excess electricity and excess heat available as low-pressure steam, $\eta_{H_{2,eq}}$, can be utilized, which is not considered as a reasonable scenario. The difference in the thermodynamic performance between case A and case OM was more pronounced in **Paper II** in relation to **Paper I**.

When evaluating case CM, it can be observed that the results are generally similar to those presented for case OM. There are minor differences in the bed-to-tube heat transfer and the NG consumption increases only slightly, with the result being a lower hydrogen production efficiency compared to case OM. However, the hydrogen production efficiency is still higher than the efficiency of the conventional SMR plant. This indicates that case CM, based on the thermodynamic assessment, is a very interesting process with net zero CO_2 emissions.

Case CB, which is based on the use of biomass as supplementary fuel presents a process which differs to a significant extent to the other cases. The hydrogen yield is significantly higher in this plant, which results in a reduced demand for NG feed to the reformer tubes to produce the targeted amount of hydrogen and a lower thermal input from the off-gas. The hydrogen production efficiency is lower in this process compared to the other cases. This is to a large extent connected to the biomass fuel which has a lower heating value. This in turn results in a higher demand for fuel supply to reach the targeted furnace temperature. The combination of reducing the NG feed and increasing the supplementary fuel feed stream with biomass allows for a higher degree of replacement with biomass since the thermal input from the off-gas is lower in case CB. The result is significant negative emissions from the plant which is probably the most interesting feature of this process.

5.2 Economic evaluation

Based on the thermodynamic performance of the three processes OM, CM and CB, the economics should also be evaluated for these systems. The economic assessment of case A and OM is presented in **Paper II** and case CM and CB are included in **Paper III**. The possibility to export electricity and heat was considered to have no economic value in this investigation. The key results of the economic assessment are presented in Table 8.

***Table 8**: Cost comparison between the two plants.*

Hydrogen production process		Case A	Case OM	Case CM	Case CB
Bare Erected Cost (M€ (% of total Bare Erected Cost, BEC))					
Desulfurization		0.71 (0.8%)	0.71 (0.8%)	0.71 (0.7%)	0.64 (0.5%)
HT WGS reactor		5.32 (5.9%)	5.32 (5.9%)	5.32 (5.3%)	4.74 (3.5%)
LT WGS reactor					18.98 (13.9%)
Reformer furnace		8.82 (9.7%)	10.88 (12.0%)	9.78 (9.8%)	12.30 (9.0%)
Pre-reformer		6.16 (6.8%)	6.16 (6.8%)	6.16 (6.2%)	5.42 (4.0%)
PSA unit		20.72 (22.9%)	20.72 (22.9%)	20.72 (20.8%)	20.22 (14.8%)
H_2 compressor		1.86 (2.1%)	1.86 (2.1%)	1.86 (1.9%)	1.87 (1.4%)
Air blower		-	0.28 (0.3%)	0.19 (0.2%)	0.49 (0.4%)
Steam turbine		7.79 (8.6%)	4.50 (5.0%)	4.43 (4.4%)	5.64 (4.1%)
Pump		0.24 (0.3%)	0.20 (0.2%)	0.22 (0.2%)	0.31 (0.2%)
Syngas cooling HX		10.57 (11.7%)	13.05 (14.4%)	11.62 (11.7%)	12.52 (9.2%)
Flue gas cooling HX		24.95 (27.5%)	21.78 (24.0%)	18.78 (18.9%)	26.64 (19.4%)
Cooling water system		3.44 (3.8%)	5.10 (5.6%)	9.47 (9.5%)	9.32 (8.4%)
CFB+cyclones				2.78 (2.8%)	1.83 (1.3%)
CO_2 compressor+pump				7.45 (7.5%)	8.93 (6.6%)
Air separation unit (ASU)					2.28 (1.7%)
Oxygen polishing unit + flue gas cleaning					2.20 (1.6%)
Bare Erected Cost (BEC)	M€	90.6	90.6	99.5	136.2
Total Plant Cost	M€/year	30.9	30.9	33.9	46.4
O&M fixed costs (M€ (% of total O&M fixed costs))					
Labour costs		1.20 (7.9%)	1.20 (8.7%)	1.80 (11.8%)	1.80 (8.8%)
Maintenance cost		5.34 (35.2%)	5.34 (38.7%)	5.87 (38.5%)	8.04 (39.3%)
Insurance cost		4.28 (28.2%)	4.28 (31.0%)	4.70 (30.8%)	6.43 (31.4%)
WGS catalyst		0.19 (1.2%)	0.19 (1.3%)	0.19 (1.2%)	0.93 (4.6%)
Reformer tube replacement		1.22 (8.0%)	0.61 (4.4%)	0.61 (4.0%)	0.73 (3.5%)
Pre-reformer and reformer catalyst		1.31 (8.6%)	1.31 (9.5%)	1.31 (8.6%)	1.61 (7.9%)
Desulfurization catalyst		0.33 (2.2%)	0.33 (2.3%)	0.33 (2.1%)	0.28 (1.3%)
Internal + external insulation		1.33 (8.8%)	0.56 (4.1%)	0.45 (3.0%)	0.64 (3.1%)
Total O&M fixed costs	M€/year	15.2	13.8	15.2	20.5
O&M variable costs (M€ (% of total O&M variable costs))					
Natural gas		140.2 (99.5%)	125.6 (97.7%)	130.2 (97.0%)	99.09 (81.2%)
Biomass					17.78 (14.6%)
Electricity				1.90 (1.4%)	3.40 (2.8%)
Cooling water make-up		0.06 (0%)	0.10 (0.1%)	0.26 (0.2%)	0.34 (0.3%)
Process water		0.71 (0.5%)	0.71 (0.5%)	0.69 (0.5%)	0.72 (0.6%)
Oxygen carrier make-up		-	2.1 (1.6%)	1.20 (0.9%)	0.55 (0.5%)
Cost of landfill					0.19 (0.2%)
Cost of lime & active carbon					0.21 (0.2%)
Total O&M variable cost	M€/year	140.9	128.5	134.2	122.1
Hydrogen production cost (including all the above costs)					
LCOH	$€/kg_{H_2}$	2.639	2.443	2.589	2.667
CO_2 avoidance cost compared to case A	$€/ton_{CO2}$			-4.28	2.71
CO_2 avoidance cost compared to case OM	$€/ton_{CO2}$			16.9	17.7

In a comparison between case A and OM it can be observed in Table 8 that the estimated total equipment costs for the two plants are similar. The reformer furnace is larger in case OM mainly as a result of the limitation in the gas velocity in the FBHE which results in a higher cost of this unit compared to the reference plant. The difference in unit cost is however small since the reformer tubes are estimated to make up a major share of the cost of the reformer. The steam turbines and the heat exchange surfaces are more expensive in case A in relation to case OM. The O&M fixed costs are similar for the two cases. The main reason for the difference in the levelized hydrogen production cost between case A and OM is the cost of the fuel which is 14.6 M€/year lower for case OM as a result of a higher production efficiency. The Levelized Cost of Hydrogen, LCOH, is more than 7% lower for case OM than for the conventional SMR production plant which indicates that this technology could be very interesting for large-scale hydrogen production. It is conceivable that case OM could also serve as a first step towards the integration of a chemical-looping combustion system allowing for inherent CO_2 capture (case CM) at a limited added cost.

Case CM is observed to have a higher equipment cost compared to case A and OM which to a large extent can be explained by the addition of another fluidized bed reactor, CO_2 compressor and a larger cooling water system. The fixed costs are similar to those presented for case A and OM whereas the variable costs are higher in case CM compared to case OM based on the energy penalty related to CO_2 capture but it is still clearly lower than for the conventional process (case A).

Case CB has an even higher equipment cost, significantly higher than the other cases. This is largely due to the addition of the LT WGS reactor as well as large demand for flue gas cooling and cooling water system. Additional reasons are added costs related to oxygen polishing, and flue gas cleaning. The reduction in variable costs for fuel is the reason for the levelized cost being similar to the other cases.

The levelized hydrogen production costs for case CM and CB are similar to the production cost with the conventional process even though CO_2 capture and compression work is added which shows how interesting from an economic point of view it should be to implement these processes. The estimated CO_2 avoidance cost is observed to be negative/close to zero for case CM and case CB, which is remarkably low. This is the case despite the fact that CO_2 capture and compression work is included. The CO_2 avoidance is however not as low when compared with case OM, but the incremental cost to capture CO_2 is, even with that process as reference, lower than existing technologies for CO_2 capture [12, 69-72]. This highlights the possible environmental and economic benefits with case CM and case CB in relation to the conventional plant. Two main reasons can explain why the CO_2 avoidance cost is so low in these cases:

- The fuel cost makes up a significant share of the levelized production cost (60-70% generally) which means that processes where the NG consumption could be reduced, or partially substituted with a cheaper fuel such as biomass can compensate for larger capital investments.
- One of the key benefits of chemical-looping combustion is connected to the potential of enabling a low energy penalty and a low incremental cost for CO_2 capture.

In the sensitivity analysis performed in **Paper II & III**, it was observed that the parameter which has the biggest effect on the levelized production cost is the cost of the fuel, especially when comparing case OM, CM and CB to case A which has the highest NG consumption. Case CB has in this regard an advantage since it is less sensitive to changes in the NG price. In the cost estimations it is observed that the cost of the reformer furnace is expected to be higher in all the proposed processes where FBHE units are used. This is however compensated by enabling operation with a lower fuel consumption and even if the cost of the FBHE unit including reformer tubes would be doubled in case OM, the levelized production cost is still lower than for the conventional plant. Furthermore, it should be added that it is important to maintain a high availability of the proposed plants to compete with the conventional SMR. Since almost all components are identical in the plants, the difference in availability should to a large extent depend on the operability of the reformer furnace which is difficult to assess at this stage without long term testing at a suitable scale.

The cost to replace the oxygen carrier in the processes is not negligible and cheaper bed materials could be of interest as long as a high fuel conversion can be obtained in the OCAC/CLC units. This is especially important in case CB where it can be expected that some of the volatiles are difficult to convert which could motivate the use of more expensive oxygen carriers in order to avoid expenses for oxygen polishing.

In the sensitivity analysis in **Paper II** it can also be observed that the conventional process is very sensitive to changes in the cost to emit CO_2. The levelized hydrogen production cost increases by 36.8% to 0.3233 $€/Nm^3_{H_2}$ when the cost to emit CO_2 increases from 0 to 100 €/ton. For case CM the LCOH is 0.2323 $€/Nm^3_{H_2}$, corresponding to a cost reduction of more than 28% compared to case A. The cost reduction is even more considerable for case CB compared to case A (more than 37%) when including the assumption that operation with negative emissions means an income corresponding to the amount of negative emissions obtained in the process.

5.3 Experimental investigation of OCAC in BFB

The component in the fuel gas which is considered to be the most difficult to burn is methane. The main aim of **Paper IV** was to investigate if methane and a more reactive fuel, PSA off-gas, could both be converted in the bed at moderate temperatures and to study the influence of the bed material by a comparison of silica sand and two oxygen carriers. Figure 12 presents the vertical concentration profile of methane in the dry gas at different bed temperatures for the three bed materials.

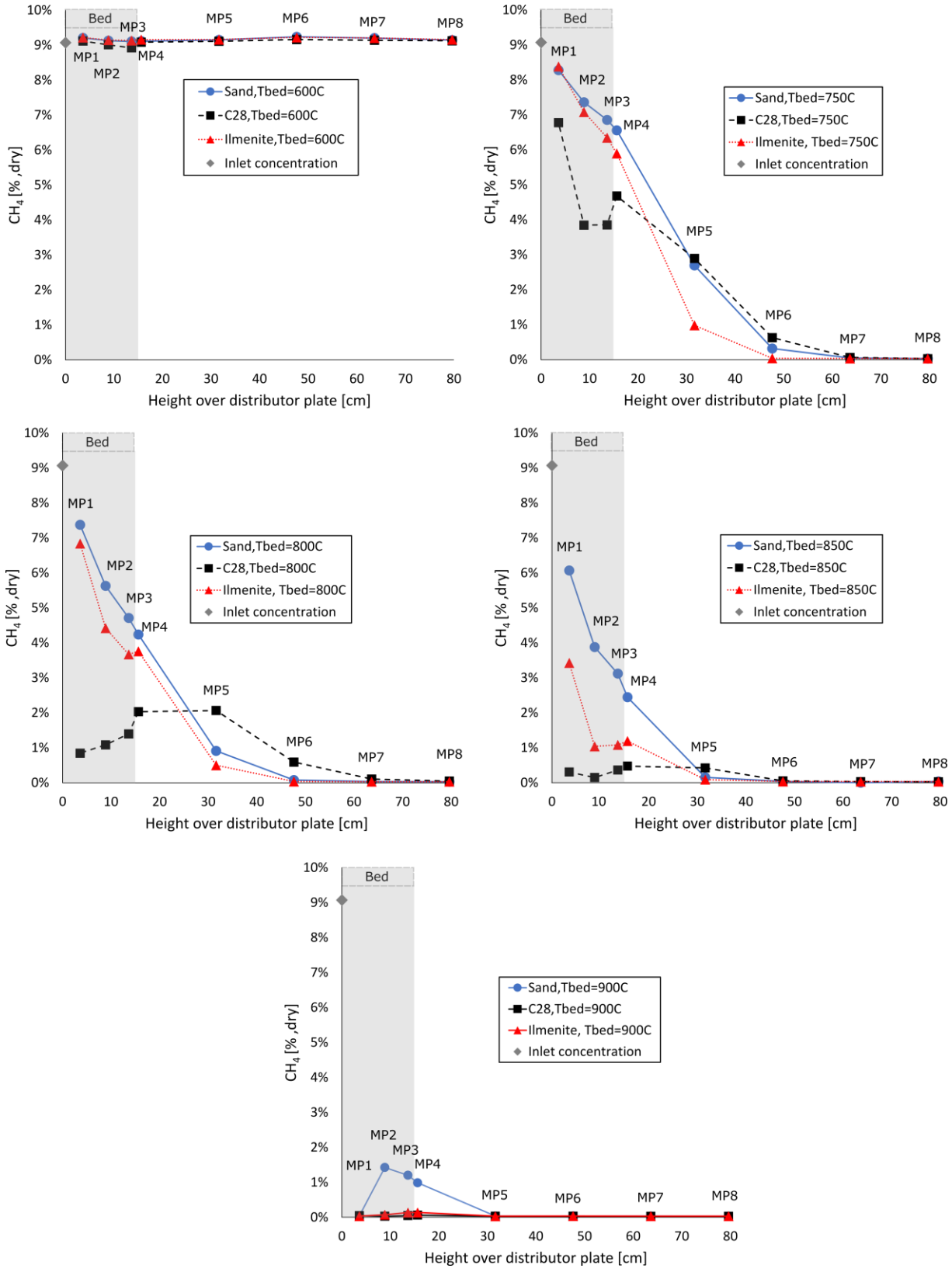

***Figure 12**: Measured gas concentration of CH_4 (in %, dry) at different distances from the distributor plate for all three bed materials where each subfigure presents a measurement at a certain bed temperature. The shadowed area indicates an approximate bed height for the three bed materials.*

It can be observed in Figure 12 that increasing furnace temperature results in a higher conversion of methane as expected. At a bed temperature of 600˚C almost no methane is converted in the

reactor but at a bed temperature of 750˚C a significant part of the methane was burnt in the bed although most of the methane conversion took place in the freeboard above the bed (above MP4). The methane was completely converted in the freeboard at bed temperatures $\geq$ 750˚C.

In the comparison between the three bed materials it can be observed that the methane concentration is overall lower in the bed when ilmenite and C28 are used as bed materials compared to sand. The difference in gas conversion can be explained by the gas-solid reaction with the oxygen carrier. This reaction only takes place in the systems with ilmenite and C28.

At the highest tested bed temperature, 900˚C, the methane conversion in the bed is close to complete with C28 and ilmenite as bed material, 99.7% and 99.3% at MP2 respectively, whereas the measured methane conversion with sand was estimated to 86.7%. The same trend can be seen at a bed temperature of 850˚C where the gas conversion is 98.7% with C28, 90.4% with ilmenite and 61.7% with sand as bed material. These experiments show that it is possible to obtain almost 100% oxidation of methane in the bed when using an oxygen carrier as bed material. This however cannot be said when using sand as material where a significant part of the gas conversion takes place above the bed at these temperatures. The measured concentrations of CO and CO_2 confirm that a reduced CH_4 concentration results in CO_2 formation corresponding to the amount of converted CH_4 with only minor CO formation corresponding to less than 1% in almost all cases.

The temperature profiles from the conducted experiments can be observed in Figure 13 which shows that the temperature drops in the freeboard in the cases where high fuel conversion takes place in the bed. The reason for this temperature drop is that the furnace temperature is below the temperature in the reactor where the exothermic reaction heats the fluidized bed reactor resulting in a heat loss to the surrounding furnace.

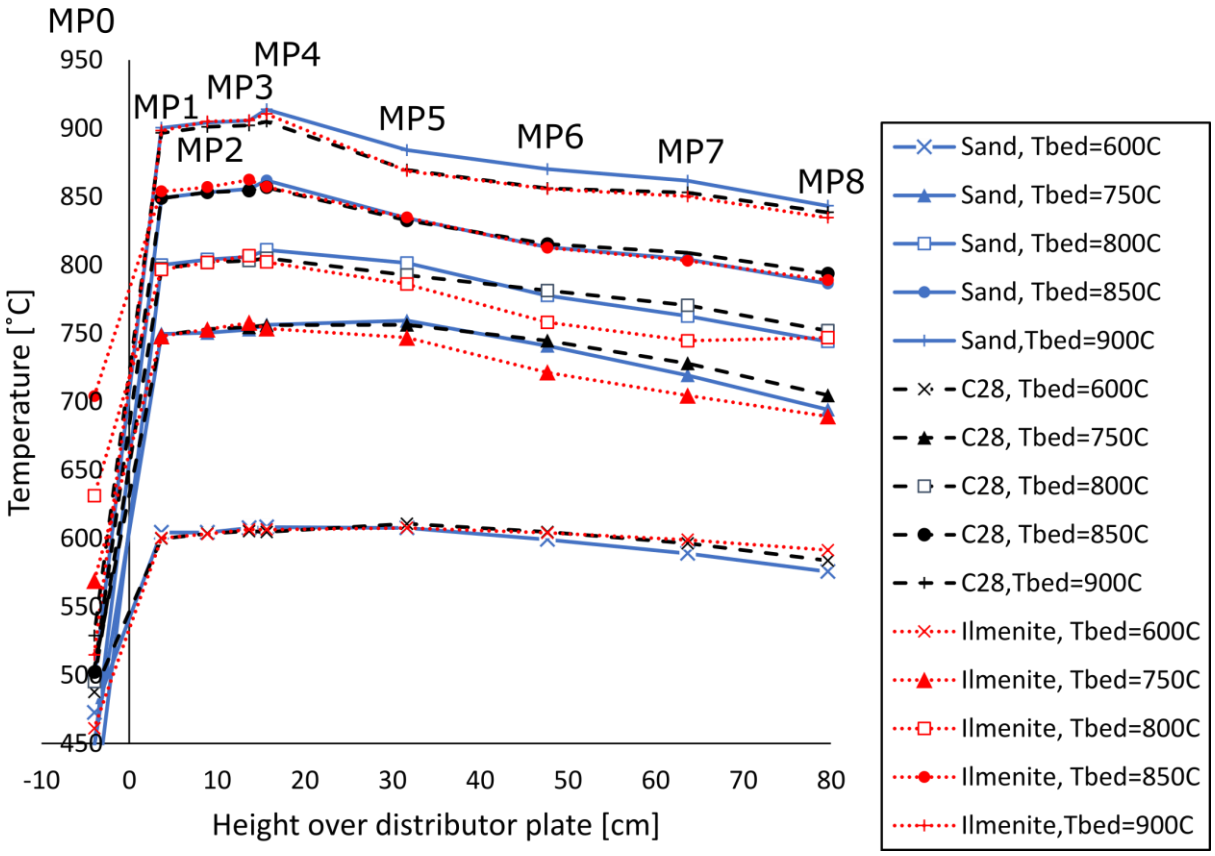

***Figure 13**: Measured temperatures at different distances from the distributor plate at five different furnace temperatures (600, 750, 800, 850 and 900˚C) for sand, C28 and ilmenite with methane as fuel.*

At a bed temperature of 750-800˚C however, the temperature change from MP4 to MP5 is more constant which can be explained by more fuel conversion taking place in the lower part of the freeboard in these cases. It can also be observed that the temperature profile is similar for the three bed materials although some differences can be observed.

In addition to measurements of CH_4, CO and CO_2, NO emissions were measured in these experiments. By comparing the results in fuel conversion and the NO concentration at 750˚C with sand as bed material compared to the results at 900˚C and C28 as bed material, several interesting observations could be made, see Figure 14.

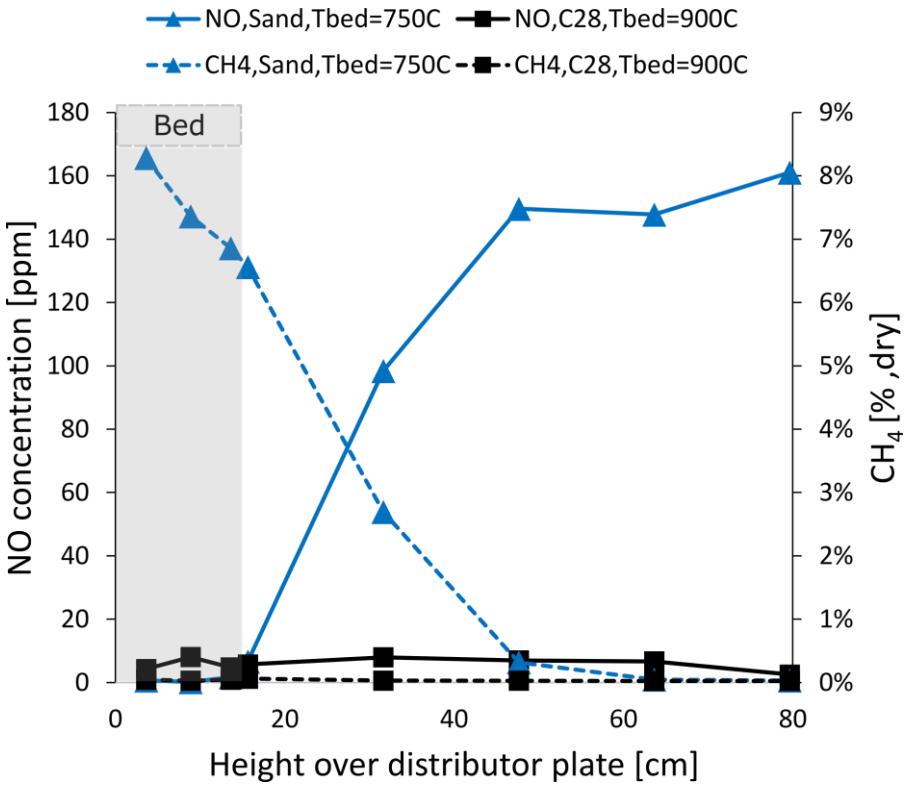

***Figure 14**: Measured dry concentrations of NO and CH_4 for sand at 750°C and at 900°C with C28 as bed material at different heights from the distribution plate. The grey area indicates approximately where the bed is located.*

With sand as bed material at 750˚C fuel conversion takes place mainly above the bed whereas with C28 the fuel is completely converted in the bed. This is apparent since the CH_4 concentration is reduced significantly between MP4 and MP5 with sand at 750˚C. Between these measurement points the NO concentration increases significantly. Thus, the NO_x formation is associated with significant fuel conversion taking place in the freeboard and causing flame combustion. The thermal inertia is low in the freeboard thus causing formation of flames and thermal NO_x since excess oxygen is available. In the bed, where the heat transfer is high between gas and solid and the thermal inertia is significant as a result of the oxygen carrier particles, no hotspots are expected. This could therefore explain why the measured NO_x concentration is so low in that zone in general. In the experiment with C28 at 900˚C almost no NO emissions are detected anywhere in the reactor. This is the case since there is no unconverted methane remaining when the gas reaches the freeboard which could otherwise lead to hotspots for NO formation.

All results for the three bed materials from the NO measurements are presented in Table 9.

***Table 9**: NO concentration (ppm, dry) at different measurement points with different bed materials and measurement points with methane as fuel.*

	Sand					Ilmenite					C28				
	600°C	750°C	800°C	850°C	900°C	600°C	750°C	800°C	850°C	900°C	600°C	750°C	800°C	850°C	900°C
MP8	0	161	51	25	11	4	255	73	17	4	3	79	10	5	3
MP7	0	148	51	NA	14	4	239	78	16	4	3	83	14	7	7
MP6	0	150	51	24	10	5	246	82	11	6	3	74	10	6	7
MP5	0	98	47	22	12	4	224	79	16	4	4	51	8	7	8
MP4	0	7	4	5	1	0	8	7	1	1	3	2	2	4	6
MP3	0	2	1	2	0	3	6	5	0	2	6	2	4	4	5
MP2	0	0	1	0	0	2	3	4	0	3	5	1	3	3	8
MP1	0	1	0	0	5	3	3	4	0	2	3	1	1	1	4

It can be observed in Table 9 that NO concentration was in general low, especially at high temperature (850-900˚C) where more fuel conversion takes place in the bed, thus resulting in less NO formation. The two main results from this experimental campaign with methane is that the use of oxygen carriers increases in-bed fuel conversion compared to using an inert bed material such as sand and that in-bed fuel conversion results in limited or no NO emissions compared to flame combustion.

When PSA off-gas was used as fuel the fuel conversion was even higher than with methane. This is not unexpected based on that methane is considered to be the most difficult fuel component to combust. This has also been shown experimentally in lab-scale tests with Fe-based oxygen carriers where the combustion efficiency was higher for PSA off-gas compared to CH_4 [43]. Significant fuel conversion took place already at the moderate temperatures with PSA off-gas as fuel and the fuel conversion in the bed was observed to increase with temperature. Only minor differences are observed between the three bed materials. In these experiments it was proven difficult to avoid ignition of the PSA off-gas in the windbox which made it difficult to perform experiments to study in-bed fuel conversion at higher temperatures. This, combined with the results for methane showing that fuel conversion increases with temperature, indicates that it should be possible to convert the PSA off-gas in the bed at the temperatures targeted for the system presented as case OM in **Papers I-III**. The NO concentrations were very low in these experiments where $\leq$ 11 ppm NO was detected at bed temperatures $\geq$ 700˚C.

The results of **Paper IV** are useful when considering the fluidized bed processes proposed in **Papers I-III**, in particular the system based on OCAC. The experiments show that it is possible to convert CH_4 in the bed which is essential for the proposed processes**.** It should however be mentioned that there are several differences between the experimental unit and the FBHE unit proposed for OCAC. First of all, the scale of the unit is much smaller than the proposed industrial scale unit. Operation with a deep bed could increase the risk of poor gas-solids contact in general due to bubble growth. Bubble size could however be reduced by use of internals in form of small horizontal tubes or packing material [73]. Secondly, the temperature in the proposed FBHE is higher which is expected to provide even higher fuel conversion in the bed. The assumptions used in **Papers I-III**, that a high fuel conversion can be expected to enable a transfer of the heat of combustion to the reformer tubes, are reasonable based on the experimental results in **Paper IV**.

5.4 Experimental investigation of bed-to-tube surface heat transfer in FBHE

The key reason for the improvement in hydrogen production efficiency and a lower LCOH for case OM, CM and CB in relation to case A presented in **Papers I-III** is the improvement in heat transfer to the reformer tubes. This was investigated further in **Papers V-VI**, where the results from two separate experimental campaigns at lab-scale and semi-commercial scale are presented. One of the main goals of these experimental studies was to verify that high heat transfer coefficients can be expected in a bed at the bed temperatures targeted for the proposed processes. **Paper V** includes the lab-scale experiments where six different material batches were used from three different bed materials (sand, ilmenite and LD slag). The key experiment in the mentioned verification was conducted by varying the bed temperature between 400-950˚C using a superficial gas velocity of 0.15 m/s for all bed material batches. The result can be observed in Figure 15. High bed-to-tube surface heat transfer coefficients, 768-1858 W/(m^{2}K), were observed where the heat transfer coefficient seemed to increase almost linearly with bed temperature.

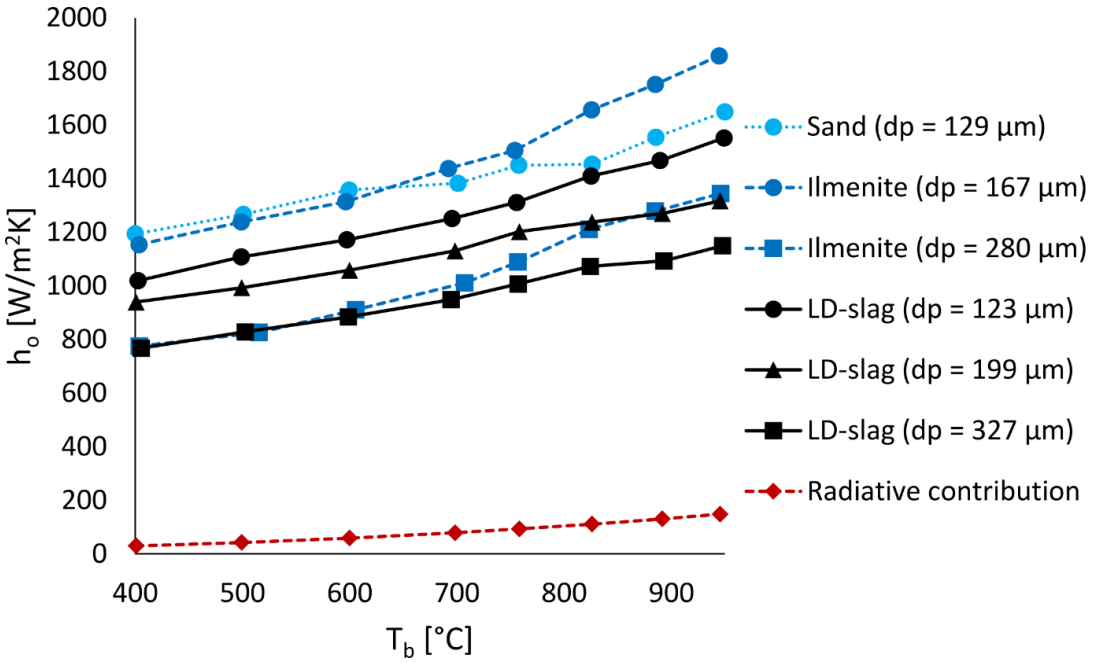

***Figure 15**: Estimated heat transfer coefficient at different bed temperatures with different bed materials and mean particle sizes, d_p.*

The effect of increasing bed temperature on bed-to-tube heat transfer is expected since the heat transfer from both radiation and convection is expected to increase with increasing bed temperature. A second observation which can be made is that the heat transfer coefficient increases with decreasing particle size. This is also expected since smaller particles are in general more efficient in exchanging heat with the tube surface. A third observation in Figure 15 is that the radiative heat transfer contribution to the overall heat transfer to the tube appears to be small although the estimated radiative heat transfer coefficient is increasing with increasing bed temperature. The estimated radiative heat transfer h_{rad} was very similar for all bed materials at a certain bed temperature where the estimated temperature on the outside of the tube was the only difference. This motivated the use of a single line in the figure indicating the radiative heat

transfer coefficient h_{rad}. The contribution from radiative heat transfer in relation to the convective heat transfer increased slightly with particle size.

The estimated heat transfer coefficients in this paper were also compared with other studies at high bed temperature to determine if it is reasonable to expect the high values found in this study. Andersson presents a review of such studies with a single tube FBHE units at high temperature where particle diameters of 465-584 μm were used and the estimated values were in the range 400-700 W/(m^2K) [74]. This indicates that the absolute values estimated in this work for the bed-to-tube heat transfer coefficient are reasonable since a significantly smaller particle size is used in the experiments in **Paper V**.

When considering the possible application of using a fluidized bed as a heat source for endothermic processes such as steam reforming, as presented in **Papers I-III**, it is important to have an adequate prediction of the bed-to-tube heat transfer coefficient. The experimentally determined heat transfer coefficients were therefore compared with heat transfer correlations. Most of the experimental research on bed-to-tube heat transfer has been done using bed temperatures below 400˚C. Since some of the most well-known heat transfer correlations have been determined at these low bed temperatures, it may be questioned if these correlations could be applicable also for higher bed temperatures. The second target of **Paper V** was therefore to evaluate if these heat transfer correlations can be applied to high bed temperature applications such as the processes based on fluidized bed heat exchangers presented in **Papers I-III**.

Heat transfer correlations were used to predict the bed-to-tube surface heat transfer coefficient for all six material batches. These values were compared with the experimentally determined values, and where the result of this comparison can be observed in Figure 16.

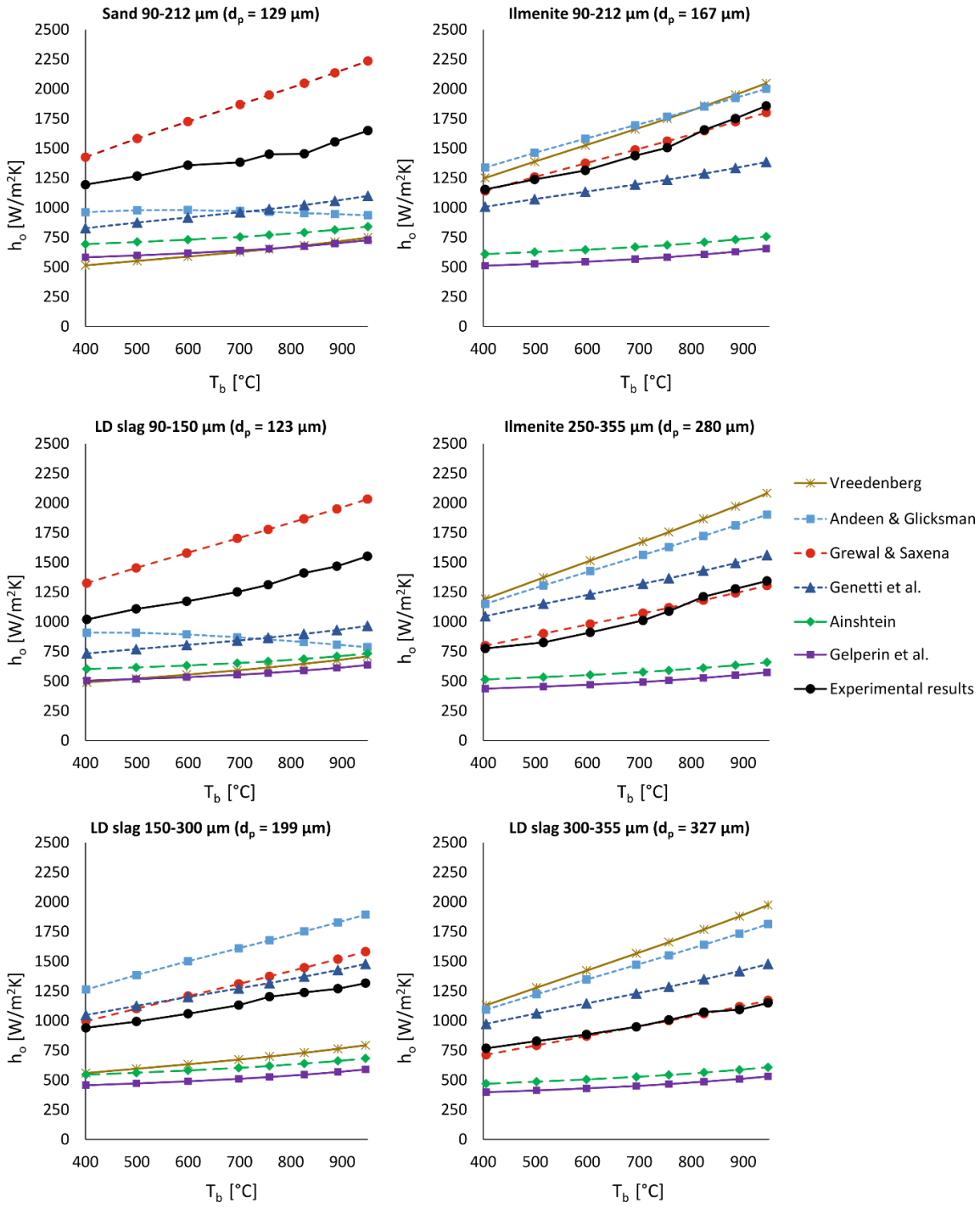

***Figure 16**: Comparison of the lab-scale experimental data with the studied correlations for each tested material batch.*

It can be observed that there is a significant spread between the heat transfer correlations. It is known to be difficult to predict the heat transfer coefficient for a varied range of experimental conditions [48] as for example a range of gas velocities. It should also be mentioned that the correlations are semi-empirical and determined at low or moderate bed temperatures and it is not obvious that these expressions can be extrapolated to determine the heat transfer coefficient also at high bed temperatures. It is therefore expected that these heat transfer correlations have difficulties to accurately estimate the heat transfer coefficient for these six material batches. All heat transfer correlations included have difficulties to predict the heat transfer coefficient accurately for the two

material batches with the smallest mean particle size. For the other four material batches it is however clear that Grewal & Saxena manages to predict the heat transfer with high accuracy. This correlation also seems to predict the effect of increasing bed temperature at a satisfactory level.

The heat transfer correlations of Grewal & Saxena and Genetti are considered to predict the bed-to-tube surface heat transfer coefficient with a high accuracy since these correlations have a Root-mean-square (RMS) error of less than 30% compared to the experimentally determined h_o. In this comparison only the convective heat transfer contribution was included so the radiative contribution was removed from both of the estimated values. The RMS error for Andeen & Glicksman was within 40% which is considered accurate. The other correlations are less accurate at predicting the bed-to-tube heat transfer coefficient in this unit.

The experimental work presented in **Paper VI** builds to a significant extent on the findings in **Paper V**. The aim of **Paper VI** was to investigate if high heat transfer coefficients can also be expected in a semi-commercial unit where a vertical U-tube is used instead of a horizontal tube. The results with sand as bed material are presented in Figure 17. A mode with high and low circulation rate was determined corresponding to 19.0 ton/h ("high circ") and 11.8 ton/h with sand, and 34.1 ("high circ") and 23.0 ton/h ("low circ") with ilmenite. Two different bed temperatures were evaluated for the two bed materials, one high which was around 850°C which is considered as a base case and one described as low at around 800°C ("low Tbed"). The fluidizing medium used on each experiment is indicated as well and for one of the experiments the U-tube was placed in parallel in relation to the particle flow instead of in perpendicular as in all other cases.

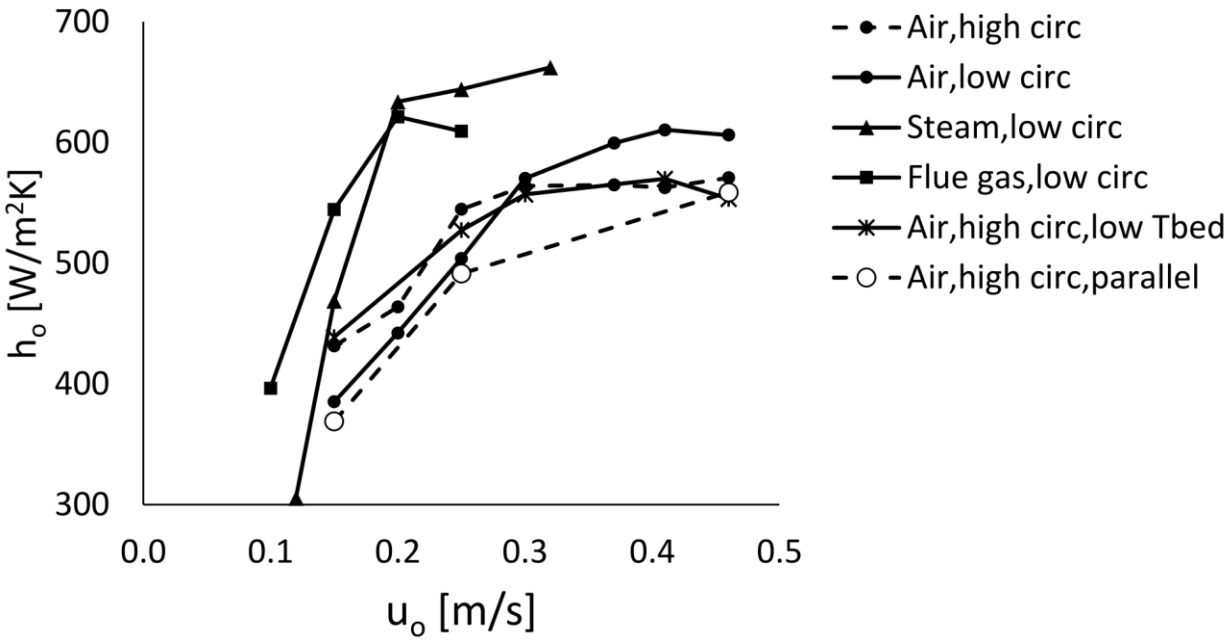

***Figure 17**: Estimated bed-to-tube heat transfer coefficient in semi-commercial scale experiment with sand as bed material at different superficial gas velocities and different process conditions.*

The estimated heat transfer coefficients are observed to be high, above 500 W/(m^{2}K), for almost all cases. This validates the observations in the lab-scale experiments both in terms of the absolute values for the bed-to-tube heat transfer, but also the expected trends with increasing heat transfer with increased fluidizing gas velocity up to a certain point when it is observed to level off.

Changes in the circulation rate and bed temperature were not observed to have a significant impact on the heat transfer within the tested ranges where the heat transfer was on average roughly 1% higher at high bed temperature and high circulation rate. A parallel orientation of the U-tube resulted in a lower heat transfer coefficient compared to using a perpendicular orientation.

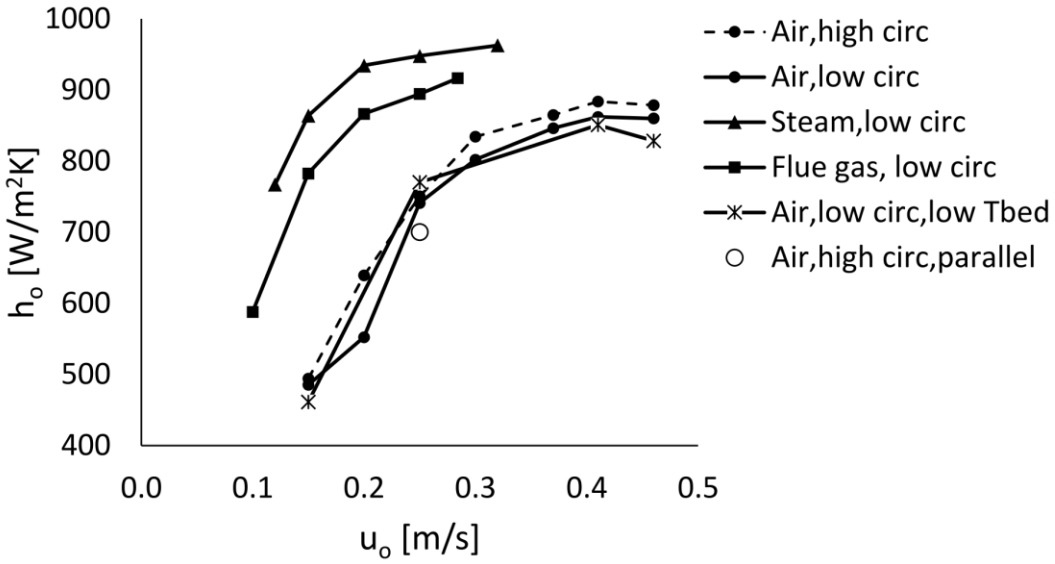

***Figure 18**: Estimated bed-to-tube heat transfer coefficient in semi-commercial scale experiment with ilmenite as bed material at different superficial gas velocities and different process conditions.*

The results with ilmenite, see Figure 18, are overall similar to those observed for sand but the absolute values are higher, around 850 rather than 550 W/(m^{2}K) for high gas velocities. The tests which were considered best for comparison between sand and ilmenite in this experiment was those where the circulation rates were the most similar and with similar bed temperatures and the same fluidizing gas, air. At a superficial gas velocity of 0.25 m/s the estimated heat transfer was 36% higher compared to the case with sand. The difference was even larger at higher superficial gas velocities. Since the particle size is of high importance when it comes to heat transfer it is difficult to claim that the improvements when comparing sand and ilmenite originate from other bed material characteristics since the ilmenite particles are smaller. It should however be said that the results here are in line with the difference seen in the lab-scale experiments. The effect of circulation rate and bed temperature was more pronounced with ilmenite as bed material where an increase in bed temperature from around 800 to 850˚C and circulation rate from 23 to 34.1 ton/h both resulted in an increase in heat transfer by around 4%.

Another interesting part of these experiments relates to the change of fluidizing gas. Based on some of the most well-known correlations for heat transfer to a horizontal tube [48-51, 53, 75] the use of steam and flue gas is predicted to result in significantly higher heat transfer coefficients than with air. This predicted change in heat transfer appears to be connected to the change in thermal conductivity and heat capacity of the gas and steam is the main contributor to this difference. The experimental results in **Paper VI** confirm these predictions where significantly higher bed-to-tube heat transfer was observed with flue gas and steam as fluidizing gas compared to using air. The predicted increase in heat transfer when changing fluidizing gas from air to flue gas was 12% on average while from air to steam a 52% increase was predicted at a bed temperature of approximately 825˚C and operating with gas velocities of 0.15, 0.2 and 0.25 m/s.

The experimental results with ilmenite were an average increase of 46% with flue gas and 58% with steam. The corresponding values for sand were 34% and 31% respectively. The experimental results were overall in line with the expected changes even though the use of flue gas as fluidizing medium resulted in a more significant improvement than expected and steam was slightly lower than the expectations. The experimental results in **Paper VI** also show that the convective heat transfer is dominating the overall heat transfer, around 85-90% of the overall heat transfer from bed to tube, which is in line with the results in **Paper V**.

The three heat transfer correlations which were the most accurate in **Paper V** were used in **Paper VI** in an attempt to verify the accuracy of these correlations also for these experiments. The main results from that comparison were that the correlation of Genetti was not accurate in the predictions while Andeen & Glicksman and Grewal & Saxena were more accurate, although the RMS error was as high as 39% and 46% respectively with ilmenite (57% and 41% with sand). This highlights once again how difficult it is to accurately predict the heat transfer coefficient in FBHE units. It should however be accentuated that the absolute values for the heat transfer coefficients estimated in both **Paper V** and **Paper VI** are in the expected range. Based on these experimental investigations it should be possible to use heat transfer correlations to predict the bed-to-tube heat transfer coefficient also for high temperature applications such as the FBHE designs for heat extraction to SMR. The assumptions used for the bed-to-tube heat transfer in the models presented in **Papers I-III** appear to be reasonable based on the results in **Papers V-VI**. As pointed out in earlier sections the idea is to use vertical tube bundles in the steam reforming application whereas a single horizontal tube and a single vertical U-tube were used in the experimental setups. This difference in tube bundle arrangement is however considered in **Papers II-III** when using heat transfer correlations to estimate the bed-to-tube surface heat transfer coefficient.

It should be mentioned that even though high heat transfer coefficients are observed for all bed materials, there are significant differences between them, especially when comparing ilmenite and the other two bed materials presented in **Paper V**. At this point, the reason for this is not well understood. This is mainly due to lack of detailed data concerning the material properties. **Paper VI** indicated also that ilmenite gives a higher heat transfer than sand but since the particle size was very different in this case it is difficult to claim that the improvement is only due to the choice of bed material. Although differences may be observed between different bed materials, high heat transfer coefficients should be expected for any bed material and the benefits from using FBHEs as a heat source for steam reforming instead of using a gas-fired furnace are considerable. Based on the high heat transfer coefficients which can be expected in FBHEs, several alternate FBHE design solutions are possible and these still obtain significant benefits compared to the conventional process, in terms of allowing for a reduction in the required flue gas temperature from the reformer furnace as presented in **Papers I-III** through a more efficient heat exchange to the reformer tubes.

6. Conclusions

This thesis evaluates three processes where fluidized bed heat exchangers are integrated in SMR plants for hydrogen production. In order to gain a comprehensive view of the suggested processes, techno-economical evaluations were combined with experimental investigations on bed-to-tube heat transfer and fluidized bed combustion.

- The results from the techno-economic assessment show that all three processes are expected to have a high performance with hydrogen production efficiencies which are 2.1-11.6% higher compared to a conventional SMR plant. The main difference is the possibility to provide a more efficient heat transfer to the reformer tubes in the fluidized bed which makes it possible to reduce fuel consumption as well as excess heat generation and CO_2 emissions.
- Two of the suggested systems integrate SMR with chemical-looping combustion, which provides inherent CO_2 capture. This can result in net zero emissions of CO_2 when using NG as supplementary fuel. When using biomass as supplementary fuel it results in a plant with significant net negative CO_2 emissions, corresponding to a reduction with 142% compared to conventional SMR plants.
- The economic evaluation of a large-scale hydrogen production plant shows that the proposed plant configurations present similar or lower levelized hydrogen production costs, ranging from a cost which is 7.1% lower to 1.4% higher compared to the conventional SMR plant. This is the case even though two of these processes include CO_2 capture and compression. The overall conclusion from this part of the work is that the processes should be of interest for industrial implementation.
- An experimental investigation of oxygen carrier aided combustion at moderate temperatures supports the hypothesis that efficient in-bed fuel conversion of the fuel gases, most notably methane, can be achieved using oxygen carriers as bed material. The methane conversion was estimated to 99.3-99.7% with the oxygen carriers compared to sand where the result was 86.7% at a bed temperature of 900°C inside the bed at a point 9 cm from the distributor plate. The results from this campaign also show that NO emissions should be reduced significantly, or almost eliminated in the plant based on FBHE compared to the conventional process.
- Two experimental investigations using high temperature FBHE reactors support the hypothesis that high heat transfer coefficients, at least above 500 W/(m^2K), can be achieved from bed to tube surface and that well-known heat transfer correlations can be used to estimate the heat transfer coefficient from bed to tube for the proposed application.

7. Reflections about project outcomes

The techno-economic analysis and experimental work with respect to fuel conversion and heat transfer measurements in this work has provided a scientific basis for the proposed process, and clearly demonstrated the viability of the concepts. It would thus be of high interest to pursue these technologies further, and below some suggestions are provided.

In regard to the techno-economic assessment it would also be interesting to compare the assessed processes with other possible hydrogen production methods with low CO_2 emissions. This should include at least two more hydrogen production processes such as SMR combined with post-combustion capture and electrolysis of water with renewable electricity. This would present a more complete overview of possible hydrogen production processes with reduced CO_2 emissions.

The assessments performed in this work show that the proposed hydrogen production concepts are interesting for large-scale implementation. However, a more detailed reactor design should be performed. Also, the construction of a pilot-scale plant to provide a proof of concept and provide a better overview of the possibilities and shortcomings of a large-scale plant. Some aspects that may put limitations in regard to process scale-up has not been evaluated in depth in this work. Both the bed height and the bed cross sectional area are greater than what is used in most industrial fluidized bed processes today. This could present challenges related to fluidization, e.g. slugging or poor gas-solid contact due to bubble formation. One possible solution to this issue could be the use of packed-fluidized beds [73, 76]. This could limit the bubble size in the bed, improve gas-solid contact with a limited detrimental effect on bed-to-tube heat transfer as well as potentially reduce the risk of pressure drop over a bed with a set bed height. Packed-fluidized beds should be evaluated in more depth to determine if these could support the implementation of the processes proposed in this thesis. It should be mentioned that the tube bundle of reformer tubes could have a similar role as the packing which therefore could limit the need for other measures to improve the gas-solid contact.

In order to avoid the risk of having poor fluidization in some parts of the cross section it could be useful to divide the fluidized bed into smaller sections divided by walls, where each section would have a separate windbox. In order to reduce the required cross section for the fluidized bed reactors it could also be possible to evaluate if the FBHE could be divided into different sections with different gas velocities, where the gas velocities are low where the tubes are present but higher in other sections to reduce the required cross section in the FBHE. This will however demand for a shorter tube pitch compared to the case with low gas velocity over the whole cross section if the same number of tube passes is used.

Another issue is the risk of erosion of tubes immersed in fluidized beds. Tube erosion is generally an issue at high gas velocities, several meters per second. Since tube erosion could be expected to be proportional to the gas velocity to the power of two at least, the risk should be limited at these low gas velocities. Nevertheless, in case erosion would be troublesome it could for example be possible to consider other tube materials than the conventional reformer tube materials. It is possible that existing CFB plants with operating FBHE units can be used to better understand the parameters which affect the lifetime of immersed tubes.

This work focused on integrating fluidized bed heat exchangers with steam reforming but there are other endothermic processes where the same technology could potentially be used. This could for example include steam cracking plants for olefins production, where hydrocarbons are cracked into different products including ethylene and propylene. The tubes where the steam cracking takes place could be heated in a fluidized bed heat exchanger instead of the traditional furnace with gas burners. Another possible application could be for calcination of limestone, where the limestone can be placed in a vessel which in turn can be placed in a fluidized bed heat exchanger instead of the traditional rotary kiln. In addition to the two examples presented here there could be other possible applications of this technology which could be evaluated for industrial implementation.

In the OCAC experiments it was shown to be difficult to avoid fuel ignition in the windbox with PSA off-gas as fuel which made it difficult to confirm that the fuel conversion took place in the bed at high bed temperatures >750°C. However, the trend at moderate temperatures show that in-bed fuel conversion takes place already at 650-700°C where roughly 50% of the CO and CH_4 gas been converted at MP4 at 650°C for example. However, in order to validate this, it would be an option to design a reactor with better gas cooling prior to entering the bed.

Additional experiments could also be used to verify which oxygen carriers are the most suitable for these processes. Based on some of the experiments performed, it seems possible that even an inert bed material could be used in the case with a single fluidized bed heat exchanger.

The reactor setup used in **Paper IV**, which makes it possible to sample gas from the reactor at different heights and depths, opens up many possibilities when it comes to evaluate in-bed fuel conversion for fluidized beds with different gas velocities, bed materials, bed inventories and fuels. A common issue when introducing solid biomass fuel to a fuel reactor in CLC systems is insufficient contact with the volatiles released from the biomass and the oxygen carrier material. This kind of setup could potentially be used to study different biomass fuel-feeding techniques such as top-feeding and in-bed-feeding where the gas concentrations measurements can be used to overview the combustion process. The results could then be used to propose a suitable method for fuel feeding in CLC systems fuelled with biomass.

The OCAC experiments show that oxygen carrier bed material can increase in-bed fuel conversion compared to using inert bed materials. It is however difficult to comment on how representative these results are for different reactor systems, bed material sizes, bed inventories and gas velocities for example. It would be interesting to perform additional experiments with more varied experimental conditions to get a better overview of the parameters which govern the in-bed fuel conversion in the BFB.

The heat transfer experiments performed within this work highlights many different opportunities. This includes both for research and for possible industrial applications. One idea is to perform a similar bed-to-tube heat transfer experiment with a whole tube bundle at industrial scale to verify the trends observed in the experiments presented here. Based on the results observed with varied fluidizing gas composition it could be investigated if flue gas should be used as fluidizing gas instead of air in external fluidized bed heat exchangers in existing industrial-scale CFB plants. Since a flue gas fan is usually available in such plants, the required changes in the process could

be quite limited. Using flue gas as fluidization gas could result in a significant improvement in heat recovery in the FBHE units, where more heat could be transferred per heat transfer area.

It would also be interesting to further study the difference between using sand and ilmenite as bed material to confirm if ilmenite can be expected to result in a higher bed-to-tube heat transfer compared to sand. The results presented in **Paper VI** also indicates that a biomass-fired CFB plant with ilmenite as bed material could operate at a higher bed temperature compared to using sand. If this is possible to achieve in existing plants, it should be possible to use higher steam data for the produced steam which in turn can enable higher plant efficiency. This assumes however that the tube material can handle a higher material temperature and that the limitation is rather on the outside of the tube in the system with sand where the risk of slagging could set an upper limit to the bed temperature. In new FBHE units it could also be possible to reduce the required heat transfer surface compared to the unit operating with sand. In addition to this, it would also be interesting to evaluate the properties of ilmenite as bed material such as heat capacity, particle emissivity and thermal conductivity to better understand how these characteristics could differ from one bed material to another.

References

[1] Smil V. Energy Transitions: Global and National Perspectives. & BP Statistical Review of World Energy. 2017.
[2] IPCC. Global Warming of 1.5°C. An IPCC Special Report on the impacts of global warming of 1.5°C above pre-industrial levels and related global greenhouse gas emission pathways, in the context of strengthening the global response to the threat of climate change, sustainable development, and efforts to eradicate poverty. World Meteorological Organization, Geneva, Switzerland. 2018. p. 32.
[3] Ogden JM. Hydrogen as an Energy Carrier: Outlook for 2010, 2030, and 2050. Institute of Transportation Studies University of California; 2004.
[4] IAEA. Hydrogen as an energy carrier and its production by nuclear power. 1999. p. 101.
[5] IEA. Technology Roadmap: Hydrogen and Fuel Cells. Paris, France, 2015.
[6] Liu K, Song C, Subramani V. Hydrogen and Syngas Production and Purification Technologies. Hoboken, New Jersey: John Wiley & Sons, Inc.; 2010.
[7] Ewan BCR, Allen RWK. A figure of merit assessment of the routes to hydrogen. International Journal of Hydrogen Energy. 2005;30:809-19.
[8] IEA. Closer look at the deployment of fuel cell EVs as of Dec. 2017. 2018.
[9] Driving Electric. Hyundai and Kia to build 500,000 hydrogen cars by 2030, https://www.drivingelectric.com/news/757/hyundai-and-kia-build-500000-hydrogen-cars-2030; 2018 [Accessed: 2019-04-13].
[10] HYBRIT. HYBRIT - Fossil-Free Steel: Summary of Findings from HYBRIT Pre-Feasibility Study 2016–2017. 2018.
[11] Stenberg V, Rydén M, Mattisson T, Lyngfelt A. Exploring novel hydrogen production processes by integration of steam methane reforming with chemical-looping combustion (CLC-SMR) and oxygen carrier aided combustion (OCAC-SMR). International Journal of Greenhouse Gas Control. 2018;74:28-39.
[12] IEAGHG. Techno-Economic Evaluation of SMR Based Standalone (Merchant) Plant with CCS. 2017.
[13] Rydén M, Lyngfelt A. Using steam reforming to produce hydrogen with carbon dioxide capture by chemical-looping combustion. International Journal of Hydrogen Energy. 2006;31:1271-83.
[14] Adánez J, Abad A, García-Labiano F, Gayán P, de Diego LF. Progress in Chemical-Looping Combustion and Reforming technologies. Progress in Energy and Combustion Science. 2012;38:215-82.
[15] Spallina V, Shams A, Battistella A, Gallucci F, Annaland MvS. Chemical Looping Technologies for H_2 Production With CO_2 Capture: Thermodynamic Assessment and Economic Comparison. Energy Procedia. 2017;114:419-28.
[16] Pans MA, Abad A, de Diego LF, García-Labiano F, Gayán P, Adánez J. Optimization of H_2 production with CO_2 capture by steam reforming of methane integrated with a chemical-looping combustion system. International Journal of Hydrogen Energy. 2013;38:11878-92.
[17] Abad A. Chemical looping for hydrogen production. In: Fennell P, Anthony, B., editor. Calcium and Chemical Looping Technology for Power Generation and Carbon Dioxide (CO_2) Capture. Cambridge, U.K: Woodhead Publishing; 2015. p. 327-67.
[18] Luo M, Yi Y, Wang S, Wang Z, Du M, Pan J, et al. Review of hydrogen production using chemical-looping technology. Renewable and Sustainable Energy Reviews. 2018;81:3186-214.

[19] Stenberg V, Spallina V, Mattisson T, Rydén M. Techno-economic analysis of processes with integration of fluidized bed heat exchangers for H2 production – Part 2: Chemical-looping combustion. Submitted for publication.
[20] Moud PH, Andersson KJ, Lanza R, Pettersson JBC, Engvall K. Effect of gas phase alkali species on tar reforming catalyst performance: Initial characterization and method development. Fuel. 2015;154:95-106.
[21] Alstrup I, Rostrup-Nielsen JR, Røen S. High temperature hydrogen sulfide chemisorption on nickel catalysts. Applied Catalysis. 1981;1:303-14.
[22] Wu H, La Parola V, Pantaleo G, Puleo F, Venezia A, Liotta L. Ni-Based Catalysts for Low Temperature Methane Steam Reforming: Recent Results on Ni-Au and Comparison with Other Bi-Metallic Systems. Catalysts. 2013;3:563-83.
[23] Rostrup-Nielsen J, Christiansen LJ. Concepts in Syngas Manufacture. London: Imperial College Press; 2011.
[24] Rath LK. Assessment of Hydrogen Production with CO_2 Capture, Volume 1: Baseline State-of-the-Art Plants. DOE/NETL-2010/1434. 2010.
[25] Carlsson M. Carbon Formation in Steam Reforming and Effect of Potassium Promotion. Johnson Matthey Technology Review. 2015;59:313-8.
[26] Boot-Handford ME, Abanades JC, Anthony EJ, Blunt MJ, Brandani S, Mac Dowell N, et al. Carbon capture and storage update. Energy & Environmental Science. 2014;7:130-89.
[27] Li J, Zhang H, Gao Z, Fu J, Ao W, Dai J. CO_2 Capture with Chemical Looping Combustion of Gaseous Fuels: An Overview. Energy & Fuels. 2017;31:3475-524.
[28] Lyngfelt A, Linderholm C. Chemical-Looping Combustion of Solid Fuels – Status and Recent Progress. Energy Procedia. 2017;114:371-86.
[29] Thunman H, Lind F, Breitholtz C, Berguerand N, Seemann M. Using an oxygen-carrier as bed material for combustion of biomass in a 12-MW_{th} circulating fluidized-bed boiler. Fuel. 2013;113:300-9.
[30] Rydén M, Hanning M, Corcoran A, Lind F. Oxygen Carrier Aided Combustion (OCAC) of Wood Chips in a Semi-Commercial Circulating Fluidized Bed Boiler Using Manganese Ore as Bed Material. Applied Sciences. 2016;6:347.
[31] Källén M, Rydén M, Lind F. Improved Performance in Fluidised Bed Combustion by the Use of Manganese Ore as Active Bed Material. 22nd International Conference on Fluidized Bed Combustion. Turku, Finland. 2015.
[32] Hallberg P, Hanning M, Rydén M, Mattisson T, Lyngfelt A. Investigation of a calcium manganite as oxygen carrier during 99h of operation of chemical-looping combustion in a 10kW_{th} reactor unit. International Journal of Greenhouse Gas Control. 2016;53:222-9.
[33] Rydén M, Jing D, Källén M, Leion H, Lyngfelt A, Mattisson T. CuO-Based Oxygen-Carrier Particles for Chemical-Looping with Oxygen Uncoupling – Experiments in Batch Reactor and in Continuous Operation. Industrial & Engineering Chemistry Research. 2014;53:6255-67.
[34] Hallberg P, Källen M, Jing D, Snijkers F, van Noyen J, Rydén M, et al. Experimental Investigation of $CaMnO_{3-\delta}$ Based Oxygen Carriers Used in Continuous Chemical-Looping Combustion. International Journal of Chemical Engineering. 2014:9.
[35] Källén M, Rydén M, Dueso C, Mattisson T, Lyngfelt A. $CaMn_{0.9}Mg_{0.1}O_{3-\delta}$ as Oxygen Carrier in a Gas-Fired 10 kW_{th} Chemical-Looping Combustion Unit. Industrial & Engineering Chemistry Research. 2013;52:6923-32.
[36] Hallberg P, Jing D, Rydén M, Mattisson T, Lyngfelt A. Chemical Looping Combustion and Chemical Looping with Oxygen Uncoupling Experiments in a Batch Reactor Using Spray-Dried $CaMn_{1-x}MxO_{3-\delta}$ (M = Ti, Fe, Mg) Particles as Oxygen Carriers. Energy & Fuels. 2013;27:1473-81.

[37] Gayán P, Pans MA, Ortiz M, Abad A, de Diego LF, García-Labiano F, et al. Testing of a highly reactive impregnated Fe_2O_3/Al_2O_3 oxygen carrier for a SR–CLC system in a continuous CLC unit. Fuel Processing Technology. 2012;96:37-47.
[38] Rydén M, Lyngfelt A, Mattisson T. $CaMn_{0.875}Ti_{0.125}O_3$ as oxygen carrier for chemical-looping combustion with oxygen uncoupling (CLOU)—Experiments in a continuously operating fluidized-bed reactor system. International Journal of Greenhouse Gas Control. 2011;5:356-66.
[39] Abad A, Adánez J, García-Labiano F, de Diego LF, Gayán P. Modeling of the chemical-looping combustion of methane using a Cu-based oxygen-carrier. Combustion and Flame. 2010;157:602-15.
[40] Chadeesingh DR, Hayhurst AN. The combustion of a fuel-rich mixture of methane and air in a bubbling fluidised bed of silica sand at 700°C and also with particles of Fe_2O_3 or Fe present. Fuel. 2014;127:169-77.
[41] Rydén M, Hanning M, Lind F. Oxygen Carrier Aided Combustion (OCAC) of Wood Chips in a 12 MW_{th} Circulating Fluidized Bed Boiler Using Steel Converter Slag as Bed Material. Applied Sciences. 2018;8:2657.
[42] Leion H, Mattisson T, Lyngfelt A. Use of Ores and Industrial Products As Oxygen Carriers in Chemical-Looping Combustion. Energy & Fuels. 2009;23:2307–15.
[43] Ortiz M, Gayán P, de Diego LF, García-Labiano F, Abad A, Pans MA, et al. Hydrogen production with CO_2 capture by coupling steam reforming of methane and chemical-looping combustion: Use of an iron-based waste product as oxygen carrier burning a PSA tail gas. Journal of Power Sources. 2011;196:4370-81.
[44] Kunii D, Levenspiel O. Fluidization Engineering (2^{nd} edition). Boston: Butterworth-Heinemann; 1991.
[45] Leckner B. Fluidized Bed Reactors: Heat and Mass Transfer. In: Michaelides E, Crowe CT, Schwarzkopf JD, editors. Multiphase Flow Handbook (second edition): CRC Press; 2017. p. 994-1029.
[46] Zhu Q. Developments in circulating fluidised bed combustion. In: Centre ICC, editor.2013.
[47] Mickley HS, Fairbanks DF. Mechanism of heat transfer to fluidized beds. AIChE Journal. 1955;1:374-84.
[48] Grewal NS, Saxena SC. Heat transfer between a horizontal tube and a gas-solid fluidized bed. International Journal of Heat and Mass Transfer. 1980;23:1505-19.
[49] Andeen BR, Glicksman LR. Heat transfer to horisontal tubes in shallow fluidized beds. ASME-AIChe Heat Transfer Conference. St Louis, MO, 1976.
[50] Genetti WE, Schmall RA, Grimmett ES. The Effect of Tube Orientation on Heat Transfer With Bare and Finned Tubes in a Fluidized Bed. Chem Engr Progr Sym Ser. 1971;116:90-6.
[51] Ainshtein VA. "An Investigation of Heat Transfer Process Between Fluidized Beds and Single Tubes Submerged in the Bed" in Zabordsky, SS., "Hydrodynamics and Heat Transfer in Fluidized Beds" MIT Press. Cambridge, Massachusetts, 1966.
[52] Gelperin, NI, Kruglikov, V, Ya., and Ainshtein, VG., in Ainshtein, VG., and Gelperin, NI., "Heat Transfer between a Fluidized Bed and a Surface," Inter Chem Engrg. 1966;6.
[53] Vreedenberg HA. Heat transfer between a fluidized bed and a horizontal tube. Chem Eng Sci,. 1958;9:52-60.
[54] Corcoran A, Knutsson P, Lind F, Thunman H. Comparing the structural development of sand and rock ilmenite during long-term exposure in a biomass fired 12MW_{th} CFB-boiler. Fuel Processing Technology. 2018;171:39-44.
[55] Berdugo Vilches T, Lind F, Rydén M, Thunman H. Experience of more than 1000h of operation with oxygen carriers and solid biomass at large scale. Applied Energy. 2017;190:1174-83.
[56] Hallberg P. PhD Thesis: Mixed Oxide Oxygen Carriers for Chemical-Looping Combustion. Gothenburg, Sweden: Chalmers University of Technology; 2017.

[57] Moldenhauer P, Hallberg P, Biermann M, Snijkers F, Albertsen K, Mattisson T, et al. Oxygen-Carrier Development of Calcium Manganite–Based Materials with Perovskite Structure for Chemical-Looping Combustion of Methane. Energy Technology. 2020;8:2000069.
[58] Lyngfelt A, Mattisson T, Rydén M, Linderholm C. 10,000 h of Chemical-Looping Combustion Operation – Where Are We and Where Do We Want to Go? 5th International Conference on Chemical Looping. Park City, Utah, USA, 2018.
[59] Moldenhauer P, Linderholm C, Rydén M, Lyngfelt A. Experimental investigation of chemical-looping combustion and chemical-looping gasification of biomass-based fuels using steel converter slag as oxygen carrier. International Conference on Negative CO_2 Emissions. Gothenburg, Sweden, 2018.
[60] Adánez J, Cuadrat A, Abad A, Gayán P, de Diego LF, García-Labiano F. Ilmenite Activation during Consecutive Redox Cycles in Chemical-Looping Combustion. Energy & Fuels. 2010;24:1402-13.
[61] Hupa M, Karlström O, Vainio E. Biomass combustion technology development – It is all about chemical details. Proceedings of the Combustion Institute. 2017;36:113-34.
[62] Martínez I, Romano MC, Chiesa P, Grasa G, Murillo R. Hydrogen production through sorption enhanced steam reforming of natural gas: Thermodynamic plant assessment. International Journal of Hydrogen Energy. 2013;38:15180-99.
[63] Turton R, Bailie RC, Whiting WB, Shaeiwitz JA. Analysis, Synthesis and Design of Chemical Processes (3rd edition), Pearson Education. 2009.
[64] Otmar Bertsch, Bertsch Energy GmbH & Co KG. Personal communication. 2018.
[65] Roberts RD, Brightling J. Maximize tube life by using internal and external inspection devices. Process Safety Progress. 2005;24:258-65.
[66] Incropera F, Dewitt D, Bergman T, Lavine A. Principles of heat and mass transfer. 7th ed. ed. Singapore, 2013.
[67] Stenberg V, Sköldberg V, Öhrby L, Rydén M. Evaluation of bed-to-tube surface heat transfer coefficient for a horizontal tube in bubbling fluidized bed at high temperature. Powder Technology. 2019.
[68] Special Metals Corporation. High Performance Alloys Literature - Inconel alloy 600. 2008.
[69] IEAGHG. Project Costs - Industrial Applications - QUEST. in CCS Cost Network - 2016 Workshop. Cambridge, Massachusetts, USA.2016.
[70] International Energy Agency. Technology Roadmap—Carbon capture and storage. 2013.
[71] Carbon Counts Company. CCS Roadmap for Industry: High-purity CO_2 sources: Final Draft Sectoral Assessment. 2010.
[72] IPCC. IPCC Special Report on Carbon Dioxide Capture and Storage. Prepared by Working Group III of the Intergovernmental Panel on Climate Change [Metz, B., O. Davidson, H. C. de Coninck, M. Loos, and L. A. Meyer (eds.)]. Cambridge, United Kingdom and New York, NY, USA2005. p. 442.
[73] Aronsson J, Krymarys E, Stenberg V, Mattisson T, Lyngfelt A, Rydén M. Improved Gas–Solids Mass Transfer in Fluidized Beds: Confined Fluidization in Chemical-Looping Combustion. Energy & Fuels. 2019;33:4442-53.
[74] Andersson B-Å. Heat transfer in stationary fluidized bed boilers. Gothenburg, Sweden: Chalmers University of Technology; 1988.
[75] Gelperin N, Kruglikov VY, Ainshtein V. Heat Transfer between a Fluidized Bed and a Surface. Inter Chem Engrg. 1966;6.
[76] Nemati N, Andersson P, Stenberg V, Rydén M. The Effect of Random Packings on Heat Transfer and particle segregation in Packed-Fluidized-Bed. Submitted for publication.